A fully integrated optimization framework for designing a complex geometry offshore wind turbine spar-type floating support structure

Mareike Leimeister[1,2], Maurizio Collu[1], and Athanasios Kolios[1]

[1]Naval Architecture, Ocean and Marine Engineering, University of Strathclyde, 100 Montrose Street, Glasgow G4 0LZ, United Kingdom
[2]Division System Technology, Fraunhofer IWES, Institute for Wind Energy Systems, Am Luneort 100, 27572 Bremerhaven, Germany

Correspondence: Mareike Leimeister (mareike.leimeister@iwes.fraunhofer.de)

Abstract. Spar-type platforms for floating offshore wind turbines are considered suitable for commercial wind farm deployment. To reduce the hurdles of such floating systems to become competitive, a fully integrated optimization framework and fully modular optimization problem setup is presented which can allow handling of many problems at various levels of fidelity. Thus, at first, a conceptual design study can shed the light on innovative floater configurations, which can, in a second step, be further optimized, utilizing the same multi-fidelity framework, to obtain detailed designs. In this paper, a spar floater for a 5 MW wind turbine is used as basis. The approach for generating an initial but very innovative floater design comprises the segmentation of the floating cylinder into three parts, the specification of a freer optimization formulation with less restrictions on the floater geometry, and the allowance for alternative ballast materials. The optimization of the support structure focuses primarily on cost reduction, expressed in terms of the objective to minimize the floater structural material. The optimization results demonstrate significant potential for cost savings when alternative structural and manufacturing strategies are considered.

Abbreviations: AEP, Annual Energy Production; ALPSO, Augmented Lagrangian Particle Swarm Optimization; BC, Base Column; BC_{low}, Base Column lower part; BC_{mid}, Base Column middle part; BC_{up}, Base Column upper part; CapEx, Capital Expenditure; COBYLA, Constrained Optimization BY Linear Approximation; DLC, Design Load Case; Dymola, Dynamic Modeling Laboratory; IWES, Institute for Wind Energy Systems; LCoE, Levelized Cost of Energy; MoWiT, Modelica library for Wind Turbines; NREL, National Renewable Energy Laboratory; NSGAII, Non-dominated Sorting Genetic Algorithm II; NSGAIII, Non-dominated Sorting Genetic Algorithm III; OC3, Offshore Code Comparison Collaboration; OC4, Offshore Code Comparison Collaboration Continuation; OpEx, Operational Expenditure; Rkfix4, Runge-Kutta fixed-step and 4th order method; RNA, Rotor-Nacelle Assembly; SPEA2, Strength Pareto Evolutionary Algorithm 2; SWL, Still Water Level; TI, Turbulence Intensity; TP, Tapered Part; UC, Upper Column

1 Introduction

With floating support structures for offshore wind turbines, more offshore wind resources can be captured and used for power generation, as around 60% to 80% of the ocean areas cannot be exploited with bottom-fixed structures, which are limited to water depths of up to around 50 m (European Wind Energy Association, 2013). The floating offshore wind technology is no longer in its infancy. Over the last decade, the technology readiness level of floating offshore wind turbine systems has significantly increased so that "floating offshore wind is coming of age", as WindEurope states in its floating offshore wind vision statement (WindEurope, 2017, p.4). The large number of research studies, research projects, scaled model tests, prototype developments, and full scale model test phases paved the way towards this current status. More than 40 floating foundation concepts exist and are under development, of which only a few are already used in small floating wind farms (Quest Floating Wind Energy, 2020; Future Power Technology, 2019; James and Ros, 2015; Mast et al., 2015). For further speed-up of the market uptake of floating offshore wind farms, significant cost-reductions are still required.

From the survey-based study by Leimeister et al. (2018) the conclusion is drawn that the spar-buoy concept is the most mature and has the highest technology readiness level, being already very convenient for volume production and certification due to its simple geometry. However, in order to enhance its suitability for multi-MW wind farm deployment, this technology has to be further advanced in order to benefit from a wider range of possible installation sites, simplified handling (both construction, assembly, transport, and installation), reduced levelized cost of energy (LCoE), as well as improved system motion performance (Leimeister et al., 2018). The advancement can be realized in a number of ways. Both Hirai et al. (2018) and Yamanaka et al. (2017) use a three-segmented advanced geometry spar, where a larger diameter column makes up the middle part to allow for shortening the overall length of the spar and reducing the system cost. In contrast, Zhu et al. (2019) utilize the three elements just in an opposite way (the spar element as middle part, interconnecting a slightly larger bottom column and a large upper column), focusing on increased restoring and improved motion performance. Within the Fukushima Floating Offshore Wind Farm Demonstration Project FORWARD an advanced spar-type support structure, consisting of a spar with a column each at the bottom, in the middle, and at the upper end, for a floating substation (Fukushima Kizuna) allows for utilization already at around 110 m water depth, improved motion performance, and reduced installation cost (Wright et al., 2019; Yoshimoto and Kamizawa, 2019; Yoshimoto et al., 2018; James and Ros, 2015; Matsuoka and Yoshimoto, 2015; Main(e) International Consulting LLC, 2013). A similarly structured advanced spar, equipped with damping fins for stabilization in sway and heave direction, was initially used for a 5 MW wind turbine (Fukushima Hamakaze), however, after some investigations and studies by Matsuoka and Yoshimoto (2015), the middle column was removed to optimize the system restoring, motion performance, and construction cost (Yoshimoto and Kamizawa, 2019; James and Ros, 2015; Main(e) International Consulting LLC, 2013). Other advancements are inspired by the oil and gas industry and deal with, for example, truss spar platforms, in which a truss section connects a bottom tank with the floating platform and heave plates can be included similarly to Fig. 1(a) (Chen et al., 2017; Perry et al., 2007; Bangs et al., 2002), or added helical strakes, as shown in Fig. 1(b), for improving the dynamic response of the floating offshore wind turbine system (Ding et al., 2017b, a). The advanced spar-type floater by the Massachusetts Institute of Technology (Lee, 2005), on the other hand, has a relatively shallow draft and gets stability support from a two-layered taut-leg

mooring system, which goes beyond a common delta or so called crowfoot connection of the mooring lines to the spar-buoy structure (Butterfield et al., 2007). Furthermore, an additional tuned mass damper (He et al., 2019) or moonpool (Fig. 1(c)) (Pham and Shin, 2019) can advance the common spar floater.

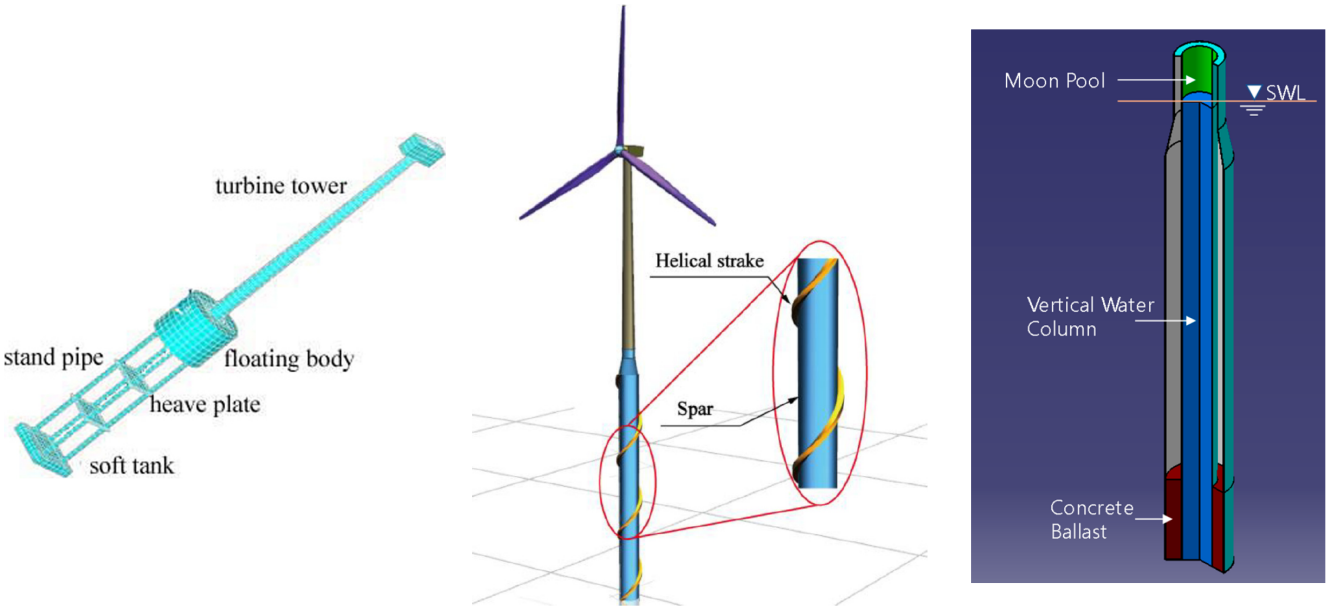

(a) Truss spar-type platform (Chen et al., 2017). (b) Added helical strakes (Ding et al., 2017a). (c) Added moonpool (Pham and Shin, 2019).

Figure 1. Inspirations for advanced spar-type floaters.

To obtain an advanced spar-type floater through optimization, most research approaches are based on the common cylindrical spar-type floater shape and utilize gradient-based methods (Dou et al., 2020; Hegseth et al., 2020; Berthelsen et al., 2012; Fylling and Berthelsen, 2011) or genetic algorithms (Karimi et al., 2017; Choi et al., 2014). Some applications are purely dealing with the support structure - focusing on basic hydrodynamic analyses, maximum system stability, and minimum material cost (Choi et al., 2014), reduced draft, weight, and cost with at the same time increased power output (Lee et al., 2015), or optimized floater cost and power generation (Gao and Sweetman, 2018) - while other design optimization approaches are highly complex and account for optimizing several components of the floating wind turbine system, such as the tower, mooring system, power cable, and/or blade-pitch controller in addition to the floating platform, and focus on extreme loads, structural strength, fatigue life, or power quality in addition to costs and global system responses (Dou et al., 2020; Hegseth et al., 2020; Sandner et al., 2014; Fylling and Berthelsen, 2011) or distinguish also between different floater types (Karimi et al., 2017; Sclavounos et al., 2008).

Even if a reduced draft is often aimed and obtained (Hegseth et al., 2020; Gao and Sweetman, 2018; Lee et al., 2015; Sandner et al., 2014) and sometimes the spar-buoy floater is subdivided into several cylindrical sections (Hegseth et al., 2020; Berthelsen et al., 2012; Fylling and Berthelsen, 2011) or a broad range of allowable values is considered for the design variables

(Karimi et al., 2017; Sclavounos et al., 2008), always common spar-type platform designs are considered, meaning a structure consisting of welded sections, for which reason even Hegseth et al. (2020) limit the maximum allowable taper angle. Thus, the aim of this paper is to demonstrate that, through a more comprehensive fully integrated design optimization approach and by allowing design variables out of a wider range of values, more potential solutions for a more innovative advanced spar-type floater design can be captured. Apart from reducing the floater draft, the main objective is cost reduction - expressed in terms of the material used - while global system performance criteria have to be fulfilled. All these requirements regarding design variables and optimization criteria are - together with specific environmental conditions and the fully coupled aero-hydro-servo-elastic dynamic characteristics of a floating offshore wind turbine system - incorporated into a fully integrated optimization framework. By means of this, a conceptual design of an innovative spar-type floating offshore wind turbine support structure design is aimed to be obtained. The focus of the optimization procedure lies on hydrodynamic and system-level analyses and not that stringent limitations on the structure and dimensions are required. This way and by considering novel structural realization approaches for the resulting optimized geometries, as well as different ballast materials, new alternatives of potential and innovative floater design solutions are opened up.

In order to figure out in detail the required characteristics of such a floating platform, first (Sect. 2), a reference floating wind turbine system with corresponding modifications and assessment criteria towards more innovative design solutions is specified. Based on this, the optimization problem - consisting of design variables, objective function, and constraints - is defined in Sect. 3. Subsequently, the automated design optimization of the advanced spar-type floating wind turbine system is performed in Sect. 4, including some preprocessing automated design load case (DLC) simulations, as well as the characterization of the automated optimization framework and the iterative optimization approach. The results of the optimization simulations are presented in Sect. 5 and further discussed in Sect. 6. Finally, some conclusions are drawn in Sect. 7.

2 Forming the basis for innovative floater configurations

According to the survey conducted by Leimeister et al. (2018), industry professionals and scientific experts judge the advanced spar-type floating platform - compared to the common spar-buoy floaters, semi-submersibles, tension leg platforms, barges, or any hybrid, multi-turbine, or mixed-energy floating system - to be the most suitable wind turbine support structure for deployment in floating offshore wind farms. To prepare the fully modular optimization problem setup, by which means problems at various levels of fidelity - such as, in this first instance, the conceptual design study on innovative floater configurations - can be addressed, both a reference floating wind turbine system (Sect. 2.1) and the advancement options, with necessary design modifications (Sect. 2.2) and associated assessment criteria (Sect. 2.3) , need to be defined.

2.1 Reference floating offshore wind turbine system

As starting point of the design optimization towards an innovative floating platform for an offshore wind turbine, a traditional spar-buoy floating wind turbine system, taken from phase IV of the OC3 (Offshore Code Comparison Collaboration) project

(Jonkman, 2010) with the main properties provided in Appendix A, is used. This is further modified, as explained in Sect. 2.2, to allow the realization of advanced features and the development of an innovative spar-type structure.

2.2 Design modifications for facilitating advancements and innovative floater configurations

An aero-hydro-servo-elastic coupled model of dynamics of the reference spar-buoy floating wind turbine system (Sect. 2.1) is developed and verified by Leimeister et al. (2020a), using MoWiT[1] (Modelica library for Wind Turbines), which is developed at Fraunhofer Institute for Wind Energy Systems IWES (Leimeister and Thomas, 2017; Thomas et al., 2014; Strobel et al., 2011). The modeling approach in MoWiT utilizes the object-oriented, equation-based, and component-based modeling language Modelica[2] and, therefore, follows a hierarchical structure with interconnected main components and subcomponents to represent the complex wind turbine system and corresponding fully coupled system dynamics in accompanying time-domain simulations. This multibody approach provides high flexibility to model various wind turbine system types, environmental conditions, and simulation settings by simply modifying single model components and, hence, forms the basis for an approach of a framework towards multi-fidelity.

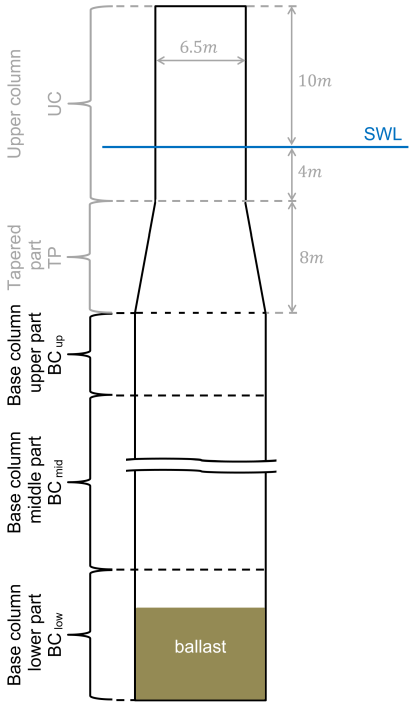

Figure 2. Geometrical definitions of the advanced spar-type floating platform.

This MoWiT model of the OC3 phase IV spar-buoy floating wind turbine system is used as basis and modified to facilitate advancements so that innovative floater designs can be obtained through automated optimization. As this work focuses on the design of the floating structure and not on the mooring system, a shorter, less heavy, and, hence, cheaper platform design shall be obtained by changing the floater geometry and allowing for further advanced features, which will be addressed in detail in Sect. 2.3. Different characteristic shapes of advanced spar-type floating platforms are pointed out in Sect. 1. In this study, a similar concept as presented by Zhu et al. (2019) and realized in the Fukushima Hamakaze floating wind turbine system (Matsuoka and Yoshimoto, 2015; Yoshimoto and Kamizawa, 2019) is applied. Thus, the long cylindrical element below the tapered part is divided into three partitions: the base column upper part $\mathrm{BC_{up}}$, which shall serve for gaining buoyancy; the base column middle part $\mathrm{BC_{mid}}$, which mainly provides the separation of the other two parts to deepen the position of part 3; and the base column lower part $\mathrm{BC_{low}}$, which can be filled with ballast and this way shall shift the center of gravity downwards.

This partitioning is schematically represented in Fig. 2, showing the unchanged geometric parameters and dimensions for the upper column (UC) and tapered part (TP) in a light shade (gray) and indicating the three sections of the base column (BC) together with the ballast filling in the base column lower part $\mathrm{BC_{low}}$.

[1] www.mowit.info (Accessed: 25 May 2021)

[2] https://www.modelica.org/ (Accessed: 22 January 2020)

Apart from these modifications, which are directly related to advancements of the geometric configuration, also the material density of the support structure and the wall thickness of the cylindrical spar-buoy elements are changed. As the material density of the OC3 phase IV spar-buoy is not explicitly stated in the definition document (Jonkman, 2010), a value of 10,000 kg/m^3 is derived in the model verification study (Leimeister et al., 2020a). However, to better match the common steel properties of offshore structures, a material density of 7,850 kg/m^3 is used in this study. Furthermore, the wall thickness of the spar[3] is changed from the fixed value of 0.0314 m, which is derived by Leimeister et al. (2020a), to a wall thickness that is adaptable to the specific floater configuration. To obtain an appropriate wall thickness for a corresponding floater design, a fixed ratio of the support structure structural mass to the displaced mass of water is deployed. This ratio is for a spar-type floating platform 0.13 - according to representative values from research designs and academic studies and excluding designs, such as the Hywind demonstrator, which are for safety reasons heavily oversized (Bachynski, 2018). Hence, the equivalent structural mass of the spar-type floater (meaning the mass of the spar-type steel structure, excluding tower, wind turbine, and ballast) with certain outer dimensions (diameters D_i and heights H_i) and corresponding displaced volume can be determined following Eq. (1).

$$\frac{\text{floater structural mass}}{\text{buoyancy mass}} = 0.13 \tag{1}$$

This results for the reference spar-buoy floating system into a structural mass of 1.070E+06 kg, which is a bit lower than the original structural mass of 1.150E+06 kg (Leimeister et al., 2020b). The corresponding appropriate wall thickness, which is kept the same for all parts of the specific floater geometry, is computed by means of Eq. (2). This equation is derived from the expression for the spar-type floater structural mass, using a material density of 7,850 kg/m^3 as explained earlier. In Eq. (2), H_i and D_i are the heights and diameters of each element, meaning UC, TP, BC_{up}, BC_{mid}, and BC_{low}. The diameter of the tapered part D_{TP}, however, is determined according to Eq. (3) as mean of the diameters of UC and BC_{up}.

$$\text{wall thickness} = \frac{\sum_i (H_i D_i) - \sqrt{\left[\sum_i (H_i D_i)\right]^2 - \frac{4}{\pi} \frac{\text{floater structural mass}}{\text{material density}} \sum_i H_i}}{2 \sum_i H_i} \tag{2}$$

$$D_{\text{TP}} = \frac{D_{\text{UC}} + D_{\text{BC,up}}}{2} \tag{3}$$

This way, a wall thickness of 0.0372 m is obtained for the original OC3 phase IV spar-buoy with reduced material density (7,850 kg/m^3) and adopted structural mass to displaced mass ratio of 0.13. This thickness value lies within the acceptable range, based on available data for the OC4 (Offshore Code Comparison Collaboration Continuation) phase II semi-submersible floater.

As the conceptual design (optimization) study does not focus on the mooring system, as already mentioned, and due to the fact that the mooring system itself could be covered in a separate or subsequent detailed design optimization task, any change in the restoring system characteristics due to shifted fairlead positions is prevented by utilizing constant (the original) resulting mooring system properties. This means that - independent of possible attachment points to the reshaped floating platform - the

[3]Referring here purely to the circumferential walls of the hollow cylindrical or conical elements, as for base and lid a fixed marginal cap thickness of 0.0001 m is applied, according to the implemented model in the verification study (Leimeister et al., 2020a).

resulting stiffness of each mooring line is taken from the system motion, assuming the original fairlead positions as defined in Sect. 2.1. A realistic mooring system design for the finally obtained optimized floating platform, which represents the considered resulting mooring system properties, can then afterwards be obtained through a subsequent optimization. This might even happen manually - depending on the degree of complexity - as it is applied in studies for designing equivalent mooring systems (Molins et al., 2015; Udoh, 2014). However, having not included the mooring system as design variable within the optimization of the spar-type floating platform, further system performance improvements due to modified mooring system parameters or fairlead positions - in addition to an optimized support structure design - are limited. This, however, leaves open the possibility of subsequent fine tuning of the conceptual design solution obtained through optimization based on hydrodynamic and system-level analyses. By addressing the mooring system in the subsequent detailed design optimization or even in a successive but separate optimization algorithm, the dynamic response of the floating offshore wind turbine system, as well as the mooring line tension itself, can be significantly improved by considering an advanced and more complex optimization problem, in which - apart from various line diameters and lengths - different mooring line arrangements and distribution forms can be utilized, the optimum number of lines within the mooring system and best fairlead position elaborated, different mooring types used or even mixed within segmented lines, and also clump weights incorporated (Tafazzoli et al., 2020; Barbanti et al., 2019; Men et al., 2019; Chen et al., 2017).

2.3 Assessment criteria towards more innovative floater design solutions

Within this study, the advancements for achieving a conceptual design of an innovative floating platform go beyond the main objectives to reduce the draft of the floater and the cost of the overall system. Further advanced features comprise the investigation of alternative materials, which are from an economic point of view comparative to currently used materials, however, positively influence the final floater design due to their different material properties and characteristics, as well as the consideration of novel structural approaches which might be more promising than the common approach of welding cylindrical and tapered sections together and allow a widening of the design space for such innovative floater shapes. In this conceptual design study, any detailed structural integrity checks are not yet addressed. However, due to the multi-fidelity model, optimization problem, and framework setup, these can be added easily for a more extensive optimization approach in a subsequent detailed design study. The advantage of focusing right now only on hydrodynamics and global system performance without defining any restrictions regarding structural aspects is that floater designs, which would have been discarded when performing structural integrity checks and as they would be unfeasible to be realized with conventional structural approaches, can still be captured as potential solutions when considering different structural realization approaches.

Thus, to achieve a shortened length of the floater, the allowable system draft is limited to the original draft of the OC3 phase IV floating wind turbine as maximum value, as well as to a recommended minimum value of 15.0 m (Ng and Ran, 2016). The resulting allowable total height of the BC (between 3.0 m and 108.0 m) has to be distributed to the three partitions; however, no restrictions prevail and also the option of utilizing not all three BC parts is possible. Thus, the minimum allowable value for the height of each of the BC parts is machine epsilon (10^{-15} m) - as a zero value is unfeasible from a modeling point of view. For the ballast height, it additionally has to be guaranteed that it does not exceed the actual $\mathrm{BC}_{\mathrm{low}}$ height.

The applied concept of a three-segmented spar-type floater with elements for buoyancy, distance, and ballast shall not only allow different heights but also different diameters of these elements. Thus, the allowable value range for the diameter of each of the BC parts is set from machine epsilon - due to the same modeling feasibility reason - to 120.0 m. The maximum diameter is chosen deliberately large - corresponding to the total maximum draft of the floating system - to ensure that the border of feasible solutions is well captured. From a manufacturing point of view, cylindrical offshore structures with diameters of more than 10.0 m are realistic: Various sources[4,5] state a value of 11.0 m, the reference semi-submersible floating platform from phase II of OC4 has an upper column diameter of 12.0 m (Robertson et al., 2014), and the diameter of the spar-buoy utilized in the Hywind Scotland floating wind farm[6,7] is even up to 14.5 m large. However, looking at other floating platform solutions, such as the Damping Pool® floater by Ideol[8] with outer dimensions of 36 m x 36 m and a resulting diagonal length of almost 51 m or again the OC4 phase II semi-submersible platform (Robertson et al., 2014) with an overall outer dimension of almost 82 m in diameter, shows that floating structures with a large overall outer diameter can be obtained without being restricted to the manufacturing feasibility limits for pure cylinders. Thus, from a hydrodynamic point of view, a cylindrical offshore structure with very large diameter can be realized as well through several smaller diameter cylinders being clustered together in a circle, representing similar hydrodynamic behavior and characteristics. Finally, attention has to be drawn on the minimum possible diameter of the BC parts, which always has to be at least as large as twice the actual wall thickness corresponding to the specific geometric floater configuration.

Having modified the diameters and heights of the three BC parts, as well as the ballast filling height, and having adjusted the wall thickness according to the structural mass to displaced mass ratio, as defined in Sect. 2.2, the ballast density has to be adjusted to match the original floating equilibrium between buoyancy force, system weight, and downward mooring force, so that the original hub height is maintained. To exclude unfeasible system solutions, in which material would have to be removed from the system (realized, for example, by reducing the material density) to meet this equilibrium condition, it has to be ensured that the actual resulting ballast density carries a positive value. However, to account for truly realistic ballast densities, also the uppermost allowable value of the ballast density has to be constrained. Leimeister et al. (2020b) have explored, within a first-stage design optimization application example, densities for common and cheap materials to be used as ballast for a floating spar-buoy. The densest material included is sandstone (or other rocks) with a density of about 2.6E+03 kg/m^3. Apart from sand, sand mixed with water, concrete, or rocks, MagnaDense (heavyweight concrete) is also used in industry as high-density material[9,10,11]. With MagnaDense, densities of up to 5.0E+03 kg/m^3 can be obtained[12] (LKAB Minerals, 2019). Even

[4] https://sif-group.com/en/wind/foundations (Accessed: 13 August 2019)

[5] https://www.windkraft-journal.de/2019/06/14/steelwind-nordenham-ist-von-wpd-die-gruendungsstrukturen-fuer-den-offshore-wind-park-yunlin-in-taiwan-zu-fertigen/136551 (Accessed: 13 August 2019)

[6] https://www.equinor.com/content/dam/statoil/documents/newsroom-additional-documents/news-attachments/brochure-hywind-a4.pdf (Accessed: 13 June 2019)

[7] https://www.equinor.com/en/news/worlds-first-floating-wind-farm-started-production.html (Accessed: 13 June 2019)

[8] https://floatgen.eu/ (Accessed: 13 August 2019)

[9] Floating offshore wind project manager at a leading company in offshore industry, personal communication, 6 February 2020.

[10] https://www.lkabminerals.com/en/industry-uses/offshore-energy/offshore-wind-structures/ (Accessed: 7 June 2020)

[11] https://www.lkabminerals.com/de/floating-offshore-wind-2018/ (Accessed: 7 June 2020)

[12] https://www.lkabminerals.com/wp-content/uploads/2019/02/MagnaDense-SDS-12-06INT-19-03.pdf (Accessed: 5 February 2020)

if minimization of the structure material volume is defined as objective function to represent the structural cost, the cost of the two potential densest ballast materials is elaborated to avoid significant larger ballast costs when utilizing MagnaDense instead of the common cheap materials pointed out by Leimeister et al. (2020b). However, when comparing the material prices for sandstone[13] (for the ballast density limit of 2.6E+03 kg/m^3) and MagnaDense[9,14] (for the ballast density limit of 5.0E+03 kg/m^3), it turns out that both ballast materials have a similar cost of around 150 $ per ton, which is less than 20% of the material cost for structural (raw) steel of about 700 $ per tonne[15] (Grogan, 2018; Butcher, 2018). Thus, the ballast density is constrained to a maximum of 5.0E+03 kg/m^3 without worrying about any negative impact on the cost situation.

As particular attention is paid to the global system performance, there are three additional criteria, which the floating offshore wind turbine system has to fulfill. For system rotational stability reasons, a maximum total inclination angle of 10.0° is allowed in operational conditions (Leimeister et al., 2020b; Katsouris and Marina, 2016; Kolios et al., 2015; Huijs et al., 2013). Furthermore, due to sensitive components in the nacelle and to prevent any issues with the lubrication, the nacelle acceleration - corresponding to the acceleration at the tower top - is commonly and depending on the specific wind turbine limited to a maximum of 0.2 to 0.3 times the gravitational acceleration constant (Nejad et al., 2017; Huijs et al., 2013; Suzuki et al., 2011); herein the lower value of 1.962 m/s^2 is used following a conservative approach (Leimeister et al., 2020b). Finally, the static translational displacement of a (non TLP-type) floating offshore wind turbine system, corresponding to the mean of the translational motion, is - based on experience - restricted to 0.2 times the water depth (320.0 m in the case of the OC3 phase IV spar-buoy floating system) and, hence, to 64.0 m in this application (Leimeister et al., 2020b).

3 Definition of the optimization problem

For obtaining a conceptual innovative floater design, following the assessment criteria - as outlined in Sect. 2.3 - and using the modified floating wind turbine system model - as described in Sect. 2.2 - as basis, an iterative optimization approach (explained in more detail in Sect. 4.3) is carried out in this study. This optimization approach requires the definition of the optimization problem - comprising the modifiable design variables x_i, the objective functions f_i to be minimized, as well as the equality (h_i) and inequality (g_i) constraints to be fulfilled - as given in formal expressions in the following:

$$
\begin{aligned}
&\text{find} && X = \{x_1, ..., x_k\} \\
&\text{to minimize} && f_i(X, system(X)) && , \; i = 1, ..., l \\
&\text{subject to} && h_i(X, system(X)) = 0 && , \; i = 1, ..., m \\
&\text{subject to} && g_i(X, system(X)) \leq 0 && , \; i = 1, ..., n
\end{aligned}
$$

The functions are either directly dependent on the design variables or also on the resulting fully coupled floating offshore wind turbine system, denoted with $system(X)$.

[13] https://www.alibaba.com/showroom/sandstone-price-per-ton.html (Accessed: 5 February 2020)
[14] https://german.alibaba.com/product-detail/magnadense-heavy-concrete–172429386.html (Accessed: 5 February 2020)
[15] https://spendonhome.com/structural-steel-fabrication-cost/ (Accessed: 5 February 2020)

3.1 Design variables

Based on the derivation of the modified spar-buoy floater model for incorporating the considered advancements (Sects. 2.2 and 2.3), the design variables vector $X = \{x_1, x_2, ..., x_6, x_7\}$ with seven ($k = 7$) elements is defined as presented in Table 1.

Table 1. Definition of the seven design variables.

Design variable	Formal expression	Description	Allowable value range	Corresponding constraints
x_1	$D_{\mathrm{BC_{up}}}$	Diameter of $\mathrm{BC_{up}}$	[10^{-15} m, 120.0 m]	g_1, g_2
x_2	$D_{\mathrm{BC_{mid}}}$	Diameter of $\mathrm{BC_{mid}}$	[10^{-15} m, 120.0 m]	g_3, g_4
x_3	$D_{\mathrm{BC_{low}}}$	Diameter of $\mathrm{BC_{low}}$	[10^{-15} m, 120.0 m]	g_5, g_6
x_4	$H_{\mathrm{BC_{up}}}$	Height of $\mathrm{BC_{up}}$	[10^{-15} m, 108.0 m]	g_7, g_8
x_5	$H_{\mathrm{BC_{mid}}}$	Height of $\mathrm{BC_{mid}}$	[10^{-15} m, 108.0 m]	g_9, g_{10}
x_6	$H_{\mathrm{BC_{low}}}$	Height of $\mathrm{BC_{low}}$	[10^{-15} m, 108.0 m]	g_{11}, g_{12}
x_7	H_{ballast}	Height of the ballast	[10^{-15} m, 108.0 m]	g_{13}, g_{14}

3.2 Objective function

As the main aim is to minimize the structural cost, just one ($l = 1$) objective function f_1 is specified (Eq. 4), which corresponds to the structure material volume of the advanced spar-type floating platform.

$$f_1 = \frac{\text{floater structural mass}}{7{,}850\ \mathrm{kg/m^3}} \tag{4}$$

3.3 Constraints

Section 2.3 covers already the assessment criteria towards more innovative floater design solutions. These make up 25 constraints, which are all specified as inequality constraints - hence, $m = 0$ (for the equality constraints h_i) and $n = 25$ (for the inequality constraints g_i) - as listed in Table 2.

4 Fully modular and automated design optimization

The final automated design optimization of the reference spar-type floating wind turbine system described in Sect. 2.2 consists of preprocessing automated system simulations for identifying the simulation conditions to be considered within the optimization (Sect. 4.1), as well as the actual iterative optimization approach for obtaining a conceptual innovative spar-type floating platform design (Sect. 4.3). Both steps utilize a framework for automated simulation and optimization developed at Fraunhofer IWES and presented in Sect. 4.2.

Table 2. Definition of the 25 inequality constraints.

Inequality constraint	Formal expression	Description
g_1	$10^{-15}\ \mathrm{m} - x_1$	Minimum allowable value of x_1
g_2	$x_1 - 120.0\ \mathrm{m}$	Maximum allowable value of x_1
g_3	$10^{-15}\ \mathrm{m} - x_2$	Minimum allowable value of x_2
g_4	$x_2 - 120.0\ \mathrm{m}$	Maximum allowable value of x_2
g_5	$10^{-15}\ \mathrm{m} - x_3$	Minimum allowable value of x_3
g_6	$x_3 - 120.0\ \mathrm{m}$	Maximum allowable value of x_3
g_7	$10^{-15}\ \mathrm{m} - x_4$	Minimum allowable value of x_4
g_8	$x_4 - 108.0\ \mathrm{m}$	Maximum allowable value of x_4
g_9	$10^{-15}\ \mathrm{m} - x_5$	Minimum allowable value of x_5
g_{10}	$x_5 - 108.0\ \mathrm{m}$	Maximum allowable value of x_5
g_{11}	$10^{-15}\ \mathrm{m} - x_6$	Minimum allowable value of x_6
g_{12}	$x_6 - 108.0\ \mathrm{m}$	Maximum allowable value of x_6
g_{13}	$10^{-15}\ \mathrm{m} - x_7$	Minimum allowable value of x_7
g_{14}	$x_7 - 108.0\ \mathrm{m}$	Maximum allowable value of x_7
g_{15}	$\max(\text{total inclination angle}) - 10.0^\circ$	Maximum total inclination angle
g_{16}	$\max(\text{horizontal nacelle acceleration}) - 1.962\ \mathrm{m/s^2}$	Maximum horizontal nacelle acceleration
g_{17}	$\text{mean}(\text{translational motion}) - 64.0\ \mathrm{m}$	Mean translational motion
g_{18}	$3.0\ \mathrm{m} - (x_4 + x_5 + x_6)$	Minimum draft
g_{19}	$x_4 + x_5 + x_6 - 108.0\ \mathrm{m}$	Maximum draft
g_{20}	$x_7 - x_6$	Ballast filling height within $\mathrm{BC_{low}}$
g_{21}	$-\text{ballast density}$	Minimum allowable value of the ballast density
g_{22}	$\text{ballast density} - 5.0\mathrm{E{+}03\ kg/m^3}$	Maximum allowable value of the ballast density
g_{23}	$0.5 \cdot 10^{-15}\ \mathrm{m} + \text{wall thickness} - 0.5x_1$	Wall thickness and diameter of $\mathrm{BC_{up}}$
g_{24}	$0.5 \cdot 10^{-15}\ \mathrm{m} + \text{wall thickness} - 0.5x_2$	Wall thickness and diameter of $\mathrm{BC_{mid}}$
g_{25}	$0.5 \cdot 10^{-15}\ \mathrm{m} + \text{wall thickness} - 0.5x_3$	Wall thickness and diameter of $\mathrm{BC_{low}}$

4.1 Preprocessing automated system simulations

Standardization and classification bodies give recommendations on DLCs to be considered when designing floating wind turbine systems. Thus, in the technical specification IEC TS 61400-3-2 (International Electrotechnical Commission, 2019b), based on the international standard IEC 61400-3-1 (International Electrotechnical Commission, 2019a), and in the standard DNVGL-ST-0119 (DNV GL AS, 2018), building on the standard DNVGL-ST-0437 (DNV GL AS, 2016), a substantial number of DLCs is listed which cover different operating states at various environmental conditions. When performing an iterative design optimization approach, however, it is not practical to simulate the full set of DLCs for each design considered. This is

not only for reasons of high computational effort, but also due to the fact that not all DLCs may be relevant or design driving for the specified optimization problem.

Thus, in this work, the same approach as taken by Leimeister et al. (2020b) in another first-stage design optimization application example is adopted. In this, first, a limited number of DLCs, critical for the considered wind turbine system and design optimization problem, is selected - a common approach in research studies (Krieger et al., 2015; Matha et al., 2014; Huijs et al., 2013; Bachynski et al., 2013; Bachynski and Moan, 2012; Suzuki et al., 2011). For the considered floating wind turbine (Sect. 2) and the corresponding optimization problem (Sect. 3) three DLCs according to IEC 61400-3-1 (International Electrotechnical Commission, 2019a) are selected: DLC 1.1 around rated wind speed (explicitly at 10.0 m/s, 11.4 m/s, and 13.0 m/s), as well as DLC 1.3 and DLC 1.6, both at 8.0 m/s, 11.4 m/s (rated wind speed), and 25.0 m/s (cut-out wind speed). These are chosen to cover highest thrust loads and corresponding system inclination and mean translational displacement at rated wind speeds, as well as maximum dynamic responses in extreme turbulent wind conditions or at severe irregular sea states, as the maximum total inclination angle, the maximum horizontal nacelle acceleration, and the mean translational motion make up three (g_{15}, g_{16}, and g_{17}) of the optimization constraints defined in Sect. 3.3, which need to be checked and adhered to.

From these selected three DLCs, 54 environmental conditions are defined, corresponding to 18 distinct environmental settings per DLC (Table 3). Thus, in each DLC, turbulent wind with three different mean wind speeds and corresponding longitudinal turbulence intensity (TI) are considered. Per wind speed, six wind seeds are taken into account to capture the randomness of turbulent wind. Three yaw misalignment angles are used and combined with two seeds each to reduce the overall number of simulation cases. The irregular sea state, prevailing in all three DLCs, is specified through the significant wave height and peak period. Furthermore, each realization of the turbulent wind with a different wind seed uses a different wave seed as well to represent the randomness of irregular waves. Finally, a current speed is specified for each wind speed.

Table 3. System parameters for preprocessing simulations of selected DLCs (Leimeister et al., 2020b).

DLC	Wind conditions				Sea conditions*		
	Wind speed	Long. TI	Wind seed	Yaw misalignment	Sign. wave height	Peak period	Current speed
1.1	10.0 m/s	18.34%	1 ... 6	-8°, 0°, 8°	1.74 m	6.03 s	0.074 m/s
	11.4 m/s	17.38%	7 ... 12	-8°, 0°, 8°	1.99 m	6.44 s	0.084 m/s
	13.0 m/s	16.53%	13 ... 18	-8°, 0°, 8°	2.30 m	6.92 s	0.096 m/s
1.3	8.0 m/s	35.00%	1 ... 6	-8°, 0°, 8°	1.44 m	5.48 s	0.059 m/s
	11.4 m/s	26.97%	7 ... 12	-8°, 0°, 8°	1.99 m	6.44 s	0.084 m/s
	25.0 m/s	16.68%	13 ... 18	-8°, 0°, 8°	4.94 m	10.14 s	0.184 m/s
1.6	8.0 m/s	20.30%	1 ... 6	-8°, 0°, 8°	10.37 m	14.70 s	0.059 m/s
	11.4 m/s	17.38%	7 ... 12	-8°, 0°, 8°	10.37 m	14.70 s	0.084 m/s
	25.0 m/s	13.64%	13 ... 18	-8°, 0°, 8°	10.37 m	14.70 s	0.184 m/s

* Please notice that each realization of the turbulent wind with a different wind seed uses a different wave seed as well.

These 54 system simulations have already been performed by Leimeister et al. (2020b) with the original OC3 phase IV floating system and are in this study carried out with the modified reference system from Sect. 2.2. The simulations are executed automatically, utilizing a fully modular framework, which is introduced in Sect. 4.2. From the total simulation time of 800 s, the last 600 s (excluding any transients at the beginning) are evaluated with respect to the system performance criteria. The results, presented by Leimeister et al. (2020b), show that DLC 1.6 at rated wind speed with wind seed number 11 and yaw misalignment angle of 8° is most critical for the total inclination angle and yields the second highest value for the horizontal nacelle acceleration, while the mean translational motion is in general far off the limit value. For the modified reference spar-type floating system, the five highest values for the three performance parameters and corresponding DLC simulation cases, as well as the position of the above described most critical DLC for the original OC3 phase IV floating wind turbine are presented in Table 4. This shows that the same DLC is still of high criticality for the modified reference spar-type floating

Table 4. The highest values for the three performance parameters and corresponding DLC simulation cases, based on the modified reference spar-type floating wind turbine system.

Position	DLC	Wind speed	Wind seed	Yaw misalignment	Max(total inclination angle)
1	1.6	11.4 m/s	8	-8°	3.924°
2	1.6	11.4 m/s	10	0°	3.876°
3	1.6	11.4 m/s	7	-8°	3.859°
4	1.6	11.4 m/s	11	8°	3.761°
5	1.6	11.4 m/s	12	8°	3.632°

Position	DLC	Wind speed	Wind seed	Yaw misalignment	Max(horizontal nacelle acceleration)
1	1.6	25.0 m/s	16	0°	2.339 m/s^2
2	1.6	25.0 m/s	14	-8°	2.322 m/s^2
3	1.6	8.0 m/s	5	8°	2.313 m/s^2
4	1.6	11.4 m/s	7	-8°	2.312 m/s^2
5	1.6	11.4 m/s	11	8°	2.311 m/s^2

Position	DLC	Wind speed	Wind seed	Yaw misalignment	Mean(translational motion)
1	1.6	11.4 m/s	9	0°	19.533 m
2	1.1	11.4 m/s	9	0°	19.455 m
3	1.3	11.4 m/s	9	0°	19.455 m
4	1.6	11.4 m/s	12	8°	19.430 m
5	1.6	11.4 m/s	8	-8°	19.351 m
6	1.6	11.4 m/s	11	8°	19.345 m

system. It scores not the highest for the performance criteria; however, the total system inclination angle is almost 96% of the highest value obtained in the 54 DLC simulations, the horizontal nacelle acceleration is even almost 99% of the highest value occurring, and the mean translational motion is just less than 1% lower than the maximum value obtained.

Thus, this DLC (DLC 1.6 at 11.4 m/s wind speed with wind seed number 11 and yaw misalignment angle of 8°) is used for defining the environmental conditions for the system simulations throughout the subsequent iterative optimization approach, which is specified in detail in Sect. 4.3. As, however, it is not ensured that the outcome of the DLC results comparison - based on the reference spar-type floating wind turbine system - does not change for the optimized floater design, the 54 environmental conditions will be simulated subsequent to the design optimization process and the criticality of the DLCs will be assessed again, as covered in Sect. 5.4.

4.2 Automated optimization framework

The preprocessing DLC simulations (Sect. 4.1), as well as the actual iterative optimization approach (Sect. 4.3), are executed in an automated manner by means of a Python-Modelica framework developed at Fraunhofer IWES (Leimeister et al., 2021, 2019). The structure and components of this framework for automated simulation and optimization are presented in Fig. 3. The framework consists of three modules: a modeling environment, a simulation tool, and a programming framework.

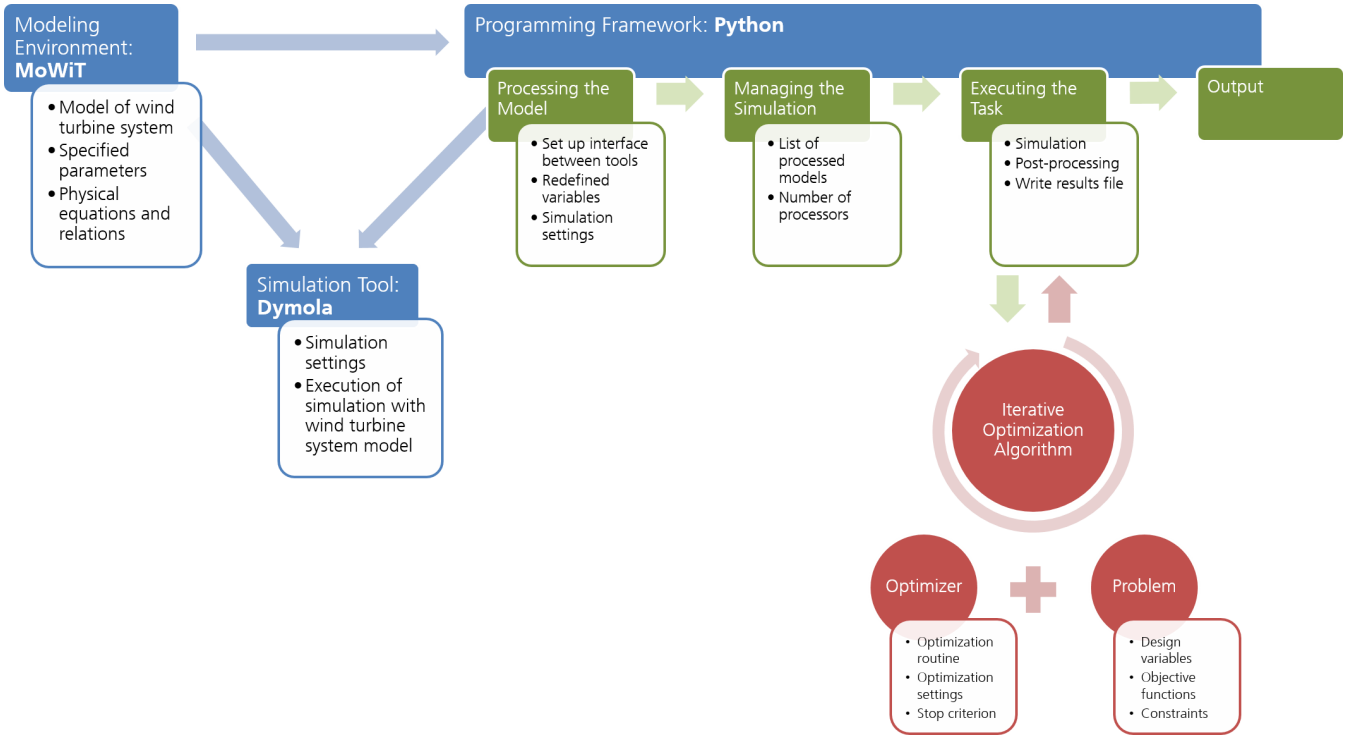

Figure 3. The Python-Modelica framework for automated simulation and optimization, adapted from Leimeister et al. (2021).

The modeling environment is MoWiT, which is already introduced in Sect. 2.2. By means of the component-based library a computational model for fully coupled aero-hydro-servo-elastic wind turbine load calculations of the system of interest is programmed in the open-source object-oriented and equation-based modeling language Modelica. The system of interest could be any state-of-the-art onshore or offshore (bottom-fixed or floating) wind turbine. In this study, the reference spar-type floating wind turbine system, described in Sects. 2.1 and 2.2, is modeled in MoWiT. Thus, system and environmental parameters, as well as the underlying physical equations and relations are specified. From the aero-, hydro-, control, and structural dynamic approaches available in MoWiT and covered in detail by Leimeister et al. (2020a), blade-element-momentum theory including dynamic stall and dynamic wake; linear Airy wave theory, Wheeler stretching, and MacCamy-Fuchs approach; built-in operating control; as well as modal reduced anisotropic beams for blades and rigid bodies for tower and floating structure, are utilized in this application.

Dymola (Dynamic Modeling Laboratory) by Dassault Systèmes[16], which is capable of time-domain simulations of complex Modelica models, is used as simulation tool. Herein, simulation and output intervals, integration settings - such as solver type, fixed integrator step size, or tolerance - as well as further specifications for translation, output, and debugging are defined.

The programming framework is coded in Python. The implemented scripts follow a four-step process. First, the interface between the three modules is established so that the provided wind turbine system model can be processed and new values can be assigned to system variables and simulation settings. This is for example done based on additional scripts for specifying the considered DLCs, so that for each of the 54 DLC simulations defined in Sect. 4.1 the respective environmental conditions (Table 3) are assigned to the corresponding model variables. Similar modifications of values of system variables are made within the iterative optimization algorithm, as explained in Sect. 4.3.3. In the second step, the model simulations are managed, as both parallel and successive execution is possible, depending on the user's preferences and the available processors. The main step is then the execution of the simulations, as well as additional post-processing scripts and documentation tasks. At this point also any iterative optimization algorithm (Sect. 4.3), defined through the optimization problem, the optimizer, and the final optimization algorithm, takes effect. Finally, the simulation results and any further specified results file are the output from the programming framework.

4.3 Specification and execution of the iterative optimization approach

As displayed in Fig. 3, the iterative optimization algorithm (Sect. 4.3.3) coupled to the Python-Modelica framework requires in addition to the model and simulation information also the definition of the optimization problem (Sect. 4.3.1) and specification of the optimizer (Sect. 4.3.2).

4.3.1 Optimization problem

The optimization problem comprises the specification of design variables, objective functions, as well as constraints. This is defined according to the details provided in Sect. 3.

[16]http://www.dymola.com/ (Accessed: 4 February 2020)

4.3.2 Optimizer

From the broad range of available algorithms and methods (Leimeister et al., 2021), only gradient-free optimization algorithms can be chosen for the application to fully coupled wind turbine systems modeled by means of MoWiT. In general, for such a complex engineering system, as a floating wind turbine is, evolutionary algorithms are highly suited to find the global optimum of a defined optimization problem (Mishra et al., 2017). From the implemented and tested optimizers NSGAII (Non-dominated Sorting Genetic Algorithm II), NSGAIII (Non-dominated Sorting Genetic Algorithm III), and SPEA2 (Strength Pareto Evolutionary Algorithm 2) - all from Platypus[17] - NSGAII is found to be the most suitable optimizer for the multi-objective optimization problem in the first-stage design optimization application example on a common floating spar-buoy wind turbine system (Leimeister et al., 2020b). As a genetic algorithm can deal with both formulations of an optimization problem (single-objective and multi-objective) and, hence, also with the optimization problem considered in this study, which holds only one objective function as defined in Sect. 3.2, and as the system simulations with the iterative optimization algorithm based on NSGAII can be also parallelized in a highly efficient manner, it is stuck to the well-performing - both with respect to the convergence speed and the compliance rate concerning the constraints - optimizer NSGAII.

For the genetic algorithm NSGAII, which follows the principle of Darwin's theory of evolution - meaning having individuals which develop further and further each generation towards performing better with respect to the fitness (objective) function -, the number of individuals in each generation (the population size), the strategies for representing the evolution, and the stop criterion for terminating the iterative optimization algorithm have to be defined.

Due to the complex optimization problem with seven design variables and 25 constraints, the population size is set equal to the maximum possible number of processors, on which simulations can be run simultaneously. On an AMD Ryzen Threadripper 2990WX 32-Core Processor with 64-bit system and 64 virtual processors 60 processors could be used for parallel simulations. Hence, 60 individuals are considered in each generation.

The individuals are randomly generated. When evaluating the objective function and constraints, the dominant individuals - each selected based on a comparison of two individuals - form the basis for the next generation, which is created without using any variator. These are the default generator, selector, and variator settings of NSGAII in Platypus.

The stop criterion for terminating the iterative optimization algorithm is defined through the total number of simulations to be performed, while the convergence is checked separately when post-processing the simulation results. As the convergence speed is not known ahead of the execution of the specific optimization problem, the experience from the first-stage design optimization application example (Leimeister et al., 2020b) is used and the total number of simulations is increased to account for the much more complex optimization problem considered in this study. Hence, the resulting number of generations being simulated is roughly tripled, so that a total number of simulations of 10,000 is chosen, corresponding to more than 166 full generations with 60 individuals each.

[17] https://platypus.readthedocs.io/en/latest/ (Accessed: 6 April 2020)

4.3.3 Optimization algorithm

Having defined and modeled the floating wind turbine system (Sects. 2.1 and 2.2), stated the simulation settings (Table 5), specified the optimization problem (Sects. 3 and 4.3.1), and selected the optimizer and corresponding parameter values (Sect. 4.3.2), the iterative optimization algorithm can be executed by means of the Python-Modelica framework for automated simulation and optimization (Sect. 4.2).

Table 5. Simulation settings.

Simulation variable	**Value**	**Note**
Simulation interval	from 0 s to 800 s	The first 200 s are accounted for as pre-simulation time to exclude any transients.
Output interval length	0.05 s	
Solver	Rkfix4	(Runge-Kutta fixed-step and 4th order method)
Fixed integrator step-size	0.01 s	

Within the iterative optimization algorithm, the values of the design variables for the 60 individuals of the first generation (number 0) are selected by the optimizer based on the specified allowable value ranges. All individuals are simulated in parallel on the available 60 processors and analyzed afterwards by the optimizer with respect to their fitness - meaning the objective function - and their compliance with the constraints based on the resulting time series, evaluated between 200 s and 800 s. As also simulations may have failed (due to too bad performance of instable floating system designs which demonstrate a negative metacentric height), the simulated time is checked against the specified simulation stop time (800 s according to Table 5). In case of an unsuccessful simulation and, hence, incomplete time series, the parameters of interest addressed in the constraints g_{15} to g_{17} for the system performance are not taken by evaluating the time series but are set equal to twice the maximum allowable value, as given in Eqs. 5 to 7. This way, it can be ensured that unsuccessful simulations do not comply with all constraints and, hence, are undesirable design solutions, which the optimizer then discards from further selection of well-performing individuals.

$$\begin{aligned} &\max(\text{total inclination angle})|_{\text{failing system}} = 2 \cdot 10.0^\circ = 20.0^\circ \\ &\quad \Rightarrow g_{15}(system(X)|_{\text{failed}}) = 20.0^\circ - 10.0^\circ = 10.0^\circ \not\leq 0 \end{aligned} \tag{5}$$

$$\begin{aligned} &\max(\text{horizontal nacelle acceleration})|_{\text{failing system}} = 2 \cdot 1.962\ \text{m/s}^2 = 3.924\ \text{m/s}^2 \\ &\quad \Rightarrow g_{16}(system(X)|_{\text{failed}}) = 3.924\ \text{m/s}^2 - 1.962\ \text{m/s}^2 = 1.962\ \text{m/s}^2 \not\leq 0 \end{aligned} \tag{6}$$

$$\begin{aligned} &\text{mean}(\text{translational motion})|_{\text{failing system}} = 2 \cdot 64.0\ \text{m} = 128\ \text{m} \\ &\quad \Rightarrow g_{17}(system(X)|_{\text{failed}}) = 128\ \text{m} - 64.0\ \text{m} = 64.0\ \text{m} \not\leq 0 \end{aligned} \tag{7}$$

Having evaluated the simulated individuals of generation 0, the optimizer selects the design variables for the individuals of the next generation (number 1), again in accordance with the specified allowable value ranges, but also based on the fitness and constraints compliance rate of each of the previous individuals, using the tournament selector for evaluating the dominance. Then, the loop of simulating the individuals, evaluating each system with respect to the objective function and constraints, and re-selecting values (from the allowable value ranges) for the design variables of the individuals of the next generation based on the performance of the individuals in the previous generation is repeated as long as the number of executed simulations is still below the specified total number of simulations of 10,000. This iterative optimization algorithm ends when the stop criterion is reached - the final results are now available.

5 Results

The optimization algorithm with the specified optimization settings is executed; however, the simulation run has to be interrupted due to a required system restart. At that time already 8,133 individuals have been simulated. To complete the specified 10,000 simulations without having any disruptive effects on the final results, the optimization is continued by providing the individuals of the last wholly simulated generation 133 as start population of the subsequent optimization execution, utilizing the operator InjectedPopulation available in Platypus. Thus, the optimization run takes effectively about 31 days and eleven hours and comprises 10,011 individuals simulated in total, ranging from generation 0 up to generation 166, with full populations up to and including generation 165.

5.1 Developments throughout the iterative optimization process

Figure 4 shows in light blue for all simulated individuals of the optimization run the values for the design variables x_1 to x_7, as defined in Sect. 3.1. The values of the design variables of the reference spar-type floating wind turbine system, covered in Sect. 2.2, are plotted additionally as red lines for comparative purposes. Post-processing of the simulation results and checking the constraints yield the dark blue recolored individuals which comply with all specified constraints. The finally selected optimum, which is presented in Sect. 5.3, is marked with a yellow filled circle framed in orange.

The developments of the design variables throughout the iterative optimization process show that in the first generations, the optimizer selects individuals covering the entire design space; however, none of the first is meeting all requirements. With more generations, the compliance rate is significantly increased, while it slightly decreases again when the focus of minimizing the objective function is coming more to the fore again. Overall, the spread in the design variables is decreased for more generations being simulated and for some design variables the change in their values is even very limited for the individuals which comply with all constraints. This indicates that the optimization algorithm is converging, though it has not yet fully converged, which is underlined by the fact that the optimum originates from the last generation.

Similarly, the developments of the constraints g_{15} to g_{25} throughout the iterative optimization process are analyzed and presented in Fig. 5. The first 14 constraints for the allowable value ranges of the design variables are excluded, as they are not constraints that are evaluated after the simulation but are taken into account ahead of the simulations when the optimizer

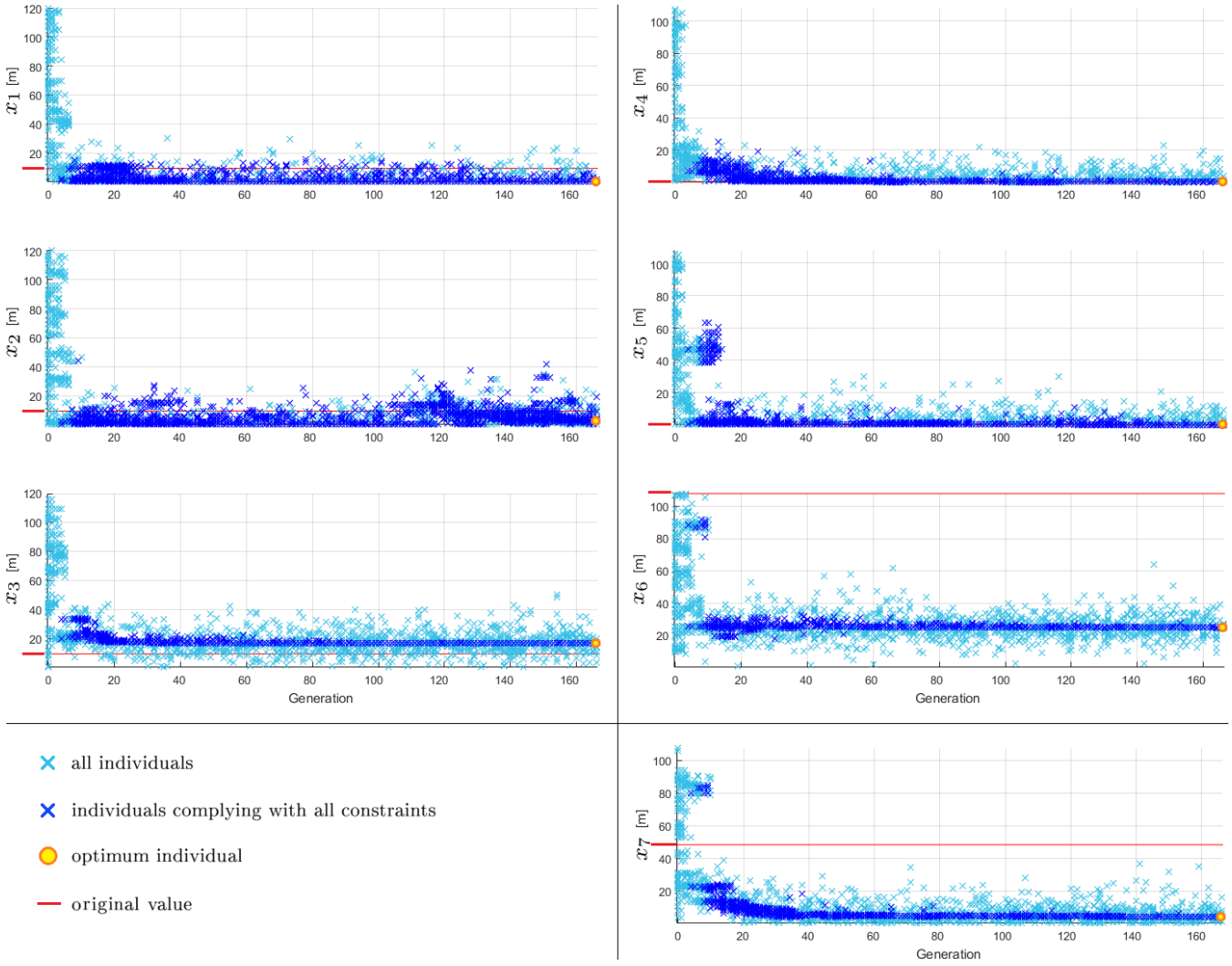

Figure 4. Development of the design variables throughout the iterative optimization process.

selects the design variables for the new individuals and, hence, are never violated. This can clearly be seen in Fig. 4, where all individuals lie within the allowable value ranges of the design variables. In Fig. 5, the light cyan crosses indicate the results for all simulated individuals, while the individuals which simultaneously comply with all constraints are recolored in dark bluish green. The limits of the inequality constraints, which should all be less or equal to zero, are indicated in red. The finally selected optimum is marked again with a yellow filled circle framed in orange. For g_{21} and g_{22} it has to be noted that the ordinate is limited to [-1E+4, 1E+4] for reasons of clarity, as a few more individuals yield values in the order of magnitude of six.

For g_{18} to g_{20} and g_{23} to g_{25}, which are directly related to and dependent on the design variables, the developments of the constraints show a similar behavior as the developments of the corresponding design variables throughout the iterative

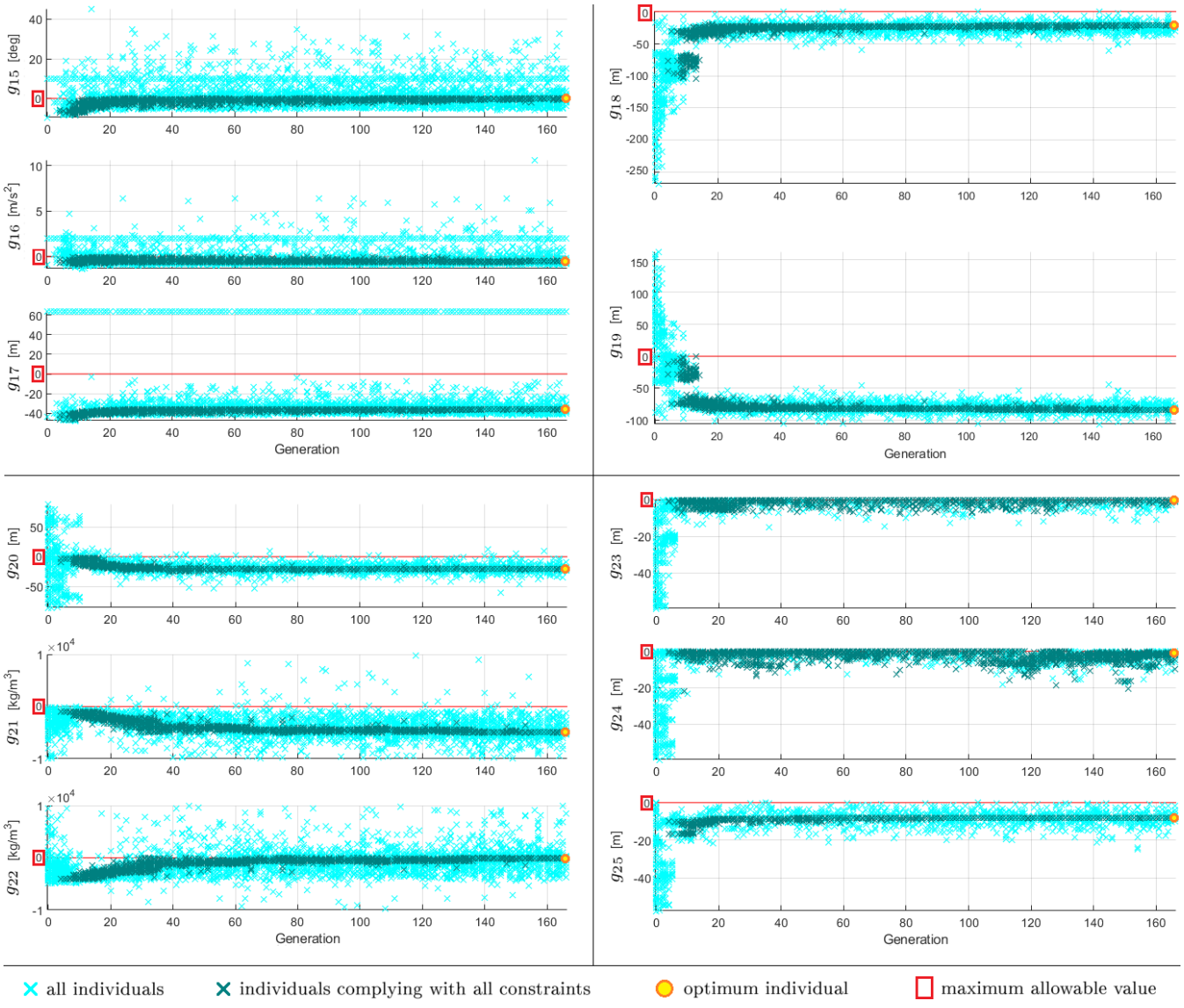

Figure 5. Development of the constraints throughout the iterative optimization process.

optimization process. For the other constraints, the trend is rather different, having a large spread in the results throughout the simulated generations. The fact that for g_{15} to g_{17} only a few distinguishable individuals are plotted in the first generations is caused by the large number of unsuccessful simulations in the first trials of the optimizer, as initially also unstable design solutions with negative metacentric height are selected and tested. Due to the failing simulations, the performance variables are set to undesired values, as explained in Sect. 4.3.3, and, hence, are all the same for all failing systems. This is as well visible throughout the generations, as there is a line at the specified undesired value formed by the individuals that do not complete the simulations successfully.

5.2 Innovative floater geometries in the design space

As presented and mentioned in Sect. 5.1, the individuals of the first generations cover the entire design space, specified through the allowable value ranges prescribed by means of the constraints g_1 to g_{14}. The individuals that comply with all constraints, however, are in a much narrower area of the design space. The geometric design variables x_1 to x_6 of these individuals, setting height and diameter of each BC part in correlation, are plotted in light blue unfilled circles in Fig. 6. The original and optimum designs are highlighted by red and blue, respectively, filled circles. From these individuals, which comply with all constraints, seven examples are selected to demonstrate the diversity of potential (meaning successful but maybe not yet optimum) innovative floater geometries. These examples are schematically drawn with black lines in Fig. 6 together with the original shape in red and having represented the ballast heights in dashed lines. The corresponding figures for design variables, performance parameters, objective function, and further resulting geometrical and structural parameters of the presented examples are outlined in Table 6. These numbers also underline that - when evaluating g_1 to g_{25} - none of the inequality constraints is violated.

Table 6. Key figures of the exemplary potential innovative floater geometries.

Ex.	Gen.	Ind.	x_1 [m]	x_2 [m]	x_3 [m]	x_4 [m]	x_5 [m]	x_6 [m]	x_7 [m]	Ballast density [kg/m^3]	Wall thickness [m]	Draft [m]
1	115	45	0.116	13.410	16.612	6.930	0.002	25.903	4.573	4.585E+03	0.0578	44.836
2	14	15	8.899	1.528	31.100	5.551	1.183	19.518	17.774	1.003E+03	0.1052	38.252
3	78	32	15.253	0.164	16.612	0.018	1.109	25.033	10.709	2.156E+03	0.0580	38.160
4	8	6	14.755	0.172	20.090	6.970	4.665	91.993	84.016	1.037E+03	0.0797	115.628
5	9	45	10.550	43.919	33.605	13.896	1.798	89.776	84.684	1.008E+03	0.1344	117.470
6	10	8	5.158	2.331	34.015	6.997	46.270	25.683	22.727	1.022E+03	0.1135	90.950
7	9	57	0.523	2.331	33.154	6.159	62.944	25.683	22.727	1.013E+03	0.1106	106.786

Ex.	Max(tot. inclination angle) [°]	Max(hor. nacelle acceleration) [m/s^2]	Mean(transl. motion) [m]	f_1 [m^3]	Steel mass [kg]	Ballast mass [kg]
1	9.9	1.337	28.155	99.1	7.778E+05	4.544E+06
2	5.0	1.231	22.241	266.2	2.090E+06	1.355E+07
3	9.3	1.724	27.308	107.7	8.455E+05	5.004E+06
4	2.6	1.955	17.503	530.1	4.162E+06	2.761E+07
5	1.6	1.664	21.089	1428.6	1.121E+07	7.570E+07
6	3.9	1.447	21.109	407.9	3.202E+06	2.111E+07
7	4.6	1.159	22.138	384.8	3.021E+06	1.987E+07

Looking at the floater geometries presented in Fig. 6, it becomes clear that not all of these shapes can be realized with conventional structural solutions, where cylindrical sections are welded together. It has to be emphasized that these results

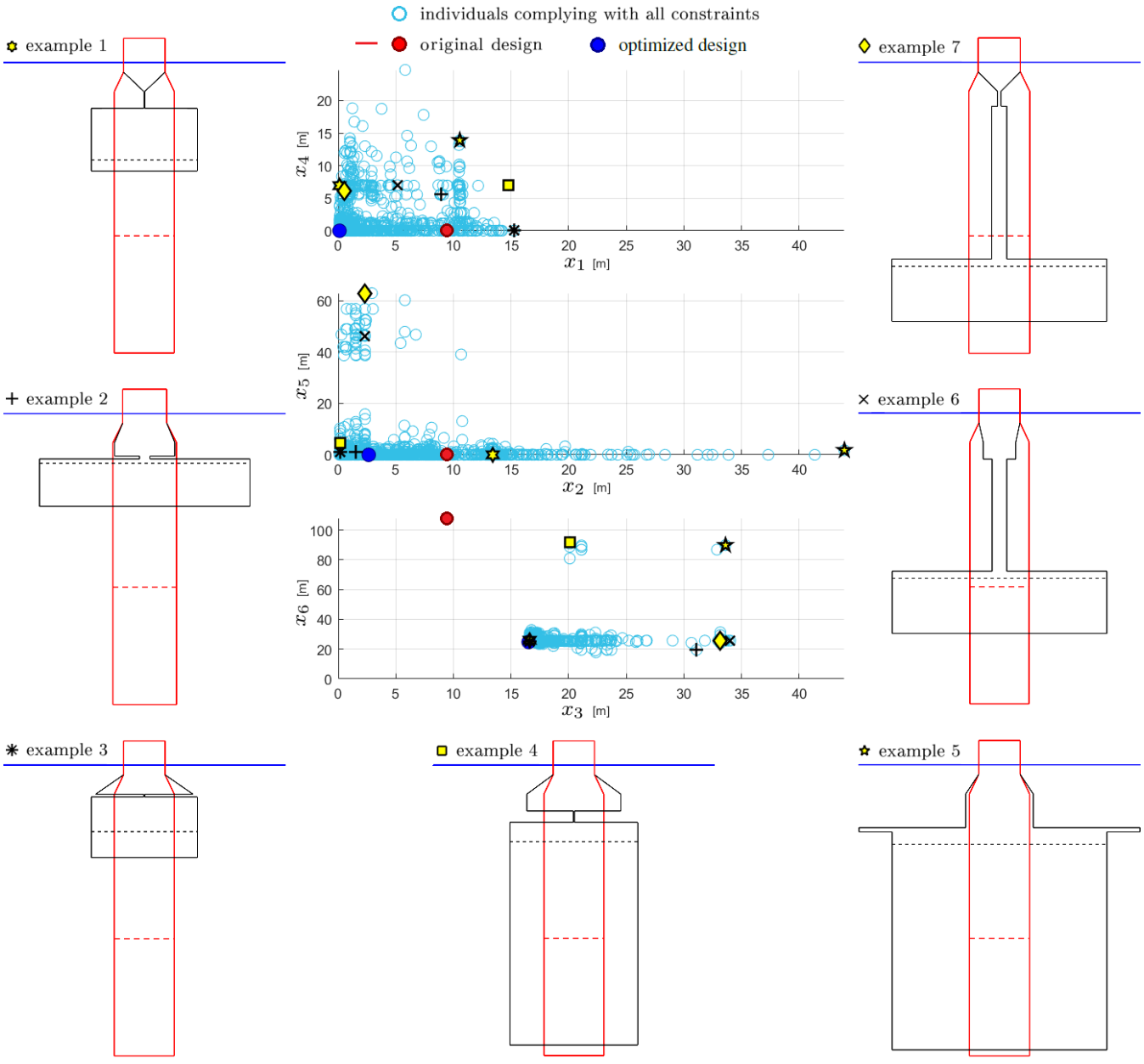

Figure 6. Exemplary potential innovative floater geometries selected from the individuals complying with all constraints.

are solely based on the hydrodynamic and system-level analyses, as specified within the optimization problem, as well as on the advancements taken into account in Sect. 2.3 which clearly intend the utilization of alternative and innovative structural realization approaches. Other additional types of analyses - addressing structural integrity, manufacturability, and localized design - can, hence, deem some of the presented potential design solutions unfeasible, which is discussed in some more

detail in Sect. 6. However, the advantage of this methodology - by focusing only on the hydrodynamics - is that a new range of potential floater designs is opened up and shapes like these presented in Fig. 6 can still be considered as feasible solutions when different structural realization approaches are applied. These approaches can range from truss structures to tendons to realize large diameter changes, as well as very thin "distance" elements, without utilizing tapered sections or having issues with the structural integrity. Idea and impulse provider for such alternative structural realization approaches can be, for example, the oil and gas industry with truss spar platform design solutions (Fig. 1(a)) (Chen et al., 2017; Perry et al., 2007; Bangs et al., 2002) or innovative floating platform concepts like the TetraSpar by Stiesdal Offshore Technologies A/S (Fig. 7(a)) (Borg et al., 2020; Stiesdal, 2019) or the pendulum-stabilized Hexafloat floater (Fig. 7(b)) by Saipem, realized in the AFLOWT project (Ribuot, 2019; Richard, 2019). Similarly to these two innovative pendulum-stabilized floating platform concepts, example 6 in Fig. 6 would suggest to implement a configuration with a separate ballast body, connected to the main body through cables or tendons. Therefore, this kind of structure cannot be realized with conventional spar manufacturing, but the approach adopted in this paper can shed the light on such innovative shapes, that may require alternative structural strategies.

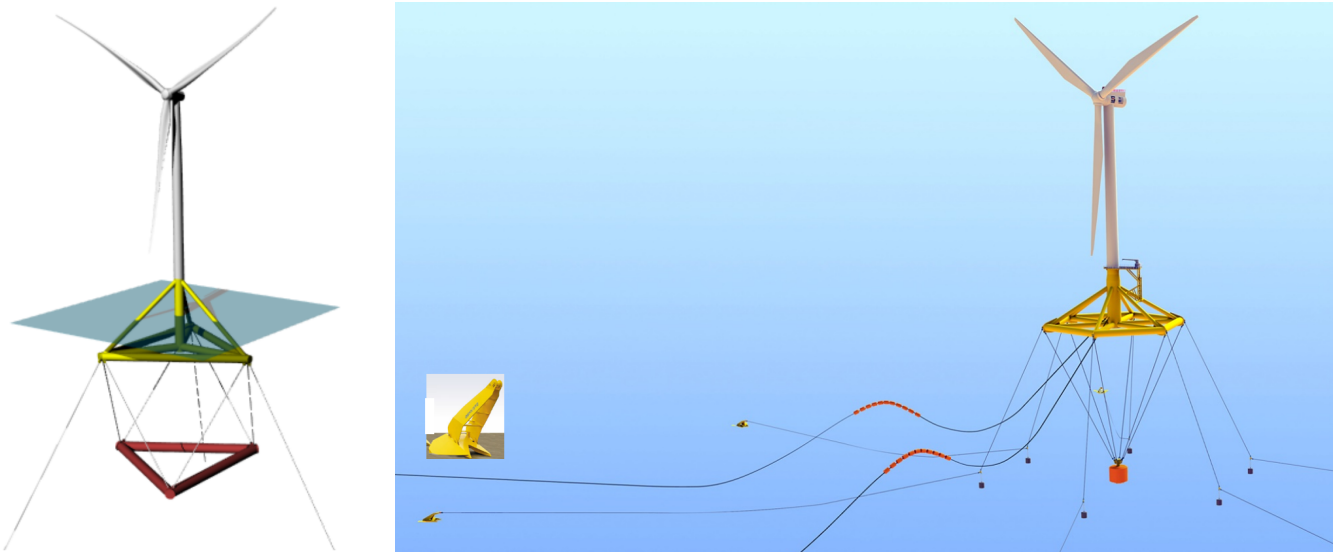

(a) Stiesdal's TetraSpar (Borg et al., 2020).

(b) Saipem's Hexafloat (Ribuot, 2019).

Figure 7. Pendulum-stabilized innovative floating platform concepts.

5.3 The optimized conceptual floater design

Due to the single-objective nature of the optimization problem, the selection of the optimum solution happens directly through evaluating the one and only objective function. This means that from all individuals that comply with all constraints, this is chosen as optimum which exhibits the lowest value for the structure material volume of its floater design solution.

First, looking at the development of the objective function f_1 throughout the iterative optimization process, as presented in Fig. 8, the trend of all simulated individuals (plotted in light green) shows a significant minimization of the objective function - clearly below the original value of 136.3 m^3, indicated in Fig. 8 by a red line - after a large spread in the first generations.

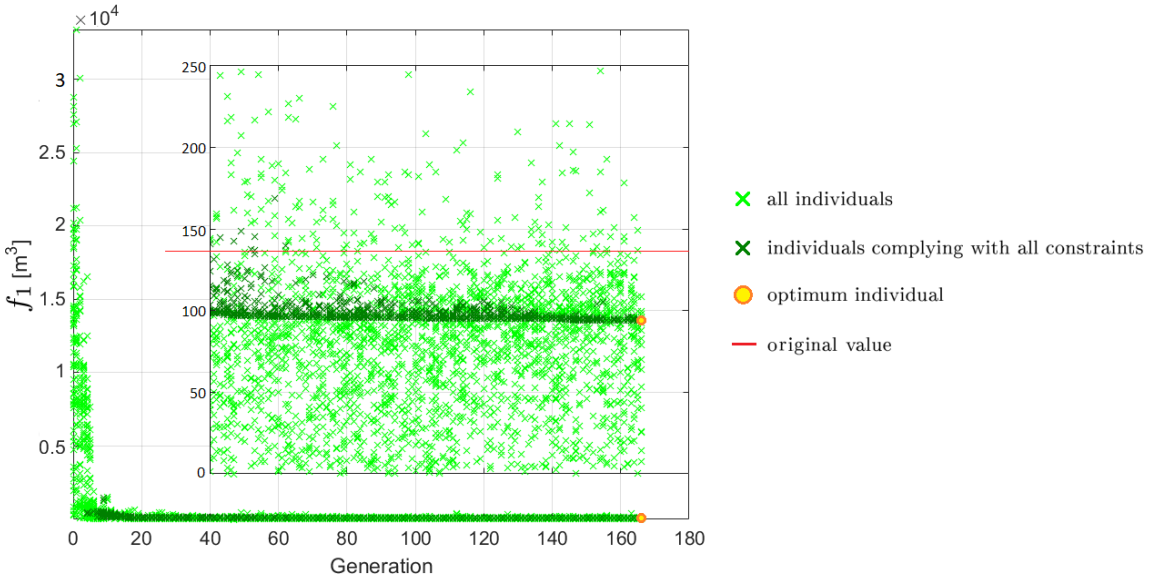

Figure 8. Development of the objective function throughout the iterative optimization process.

Zooming into the objective function results from generation 40 on, as included in Fig. 8, provides a much clearer indication of the development of the minimum structure material volume for the individuals which comply with all constraints (recolored in dark green): they aggregate to an asymptote. This is already visible in early generations; however, the spread in the objective function results of the individuals complying with all constraints is decreasing with more generations being simulated. This asymptotic clustering of the individuals which comply with all constraints to a minimum objective function value on the one hand states the convergence of the iterative optimization process and on the other hand portends that there will be several - more or less similar (elaborated in the following) - design solutions, which yield comparable low structure material volumes that are all very close to the minimum value observed.

The individual with the minimum structure material volume is pointed out in Fig. 8 by means of a yellow filled circle framed in orange. This design solution yields a reduction of the structure material volume of more than 31% compared to the original (modified) reference spar-type floating platform, for which it must be noted that it neither has been designed with the same design requirements, nor has it yet been optimized. The fact that this optimum solution is just found in the last generation simulated states that full convergence is not yet reached, despite the converging trend in most of the design variables and constraints, as well as in the objective function. Nevertheless, due to the asymptotic aggregation of the individuals mentioned above, the first ten minimum objective function results from the individuals which comply with all constraints are evaluated. This results - as some individuals yield the same objective function value - into 16 individuals with a just by 2.84E-4% increased

structure material volume, comparing the tenth lowest with the minimum value, and shapes that are difficult to distinguish from each other. This proves the above mentioned anticipation that - due to the convergence of the iterative optimization process and the aggregation of the individuals' objective function results to an asymptote - several very similar floater design solutions of comparable low structure material volumes are found. If, in addition to the maximum number of simulations, a reasonable convergence tolerance had been specified as supplementary stop criterion, the optimization algorithm would not have required all 10,000 simulations and would have stopped much earlier. However, due to the strong similarity of the last design solutions, no significant differences in the results would have been perceived.

The geometry of the optimized conceptual floater shape (black line) is shown schematically in Fig. 9 in comparison to the original floating platform drawn in red. The key figures of the optimized floater geometry are presented in Table 7. The system performance - maximum total inclination angle, maximum horizontal nacelle acceleration, and mean translational motion - points out that the maximum total inclination angle is the most critical performance criterion, as the obtained value from the optimized design is equal to the specified upper limit of 10°. With respect to the design development trend within the iterative optimization process, both Fig. 9 and Table 7 indicate the following advancements: To reduce the structure material volume, the overall length of the floating platform is significantly decreased compared to the original geometry (the draft of the optimized

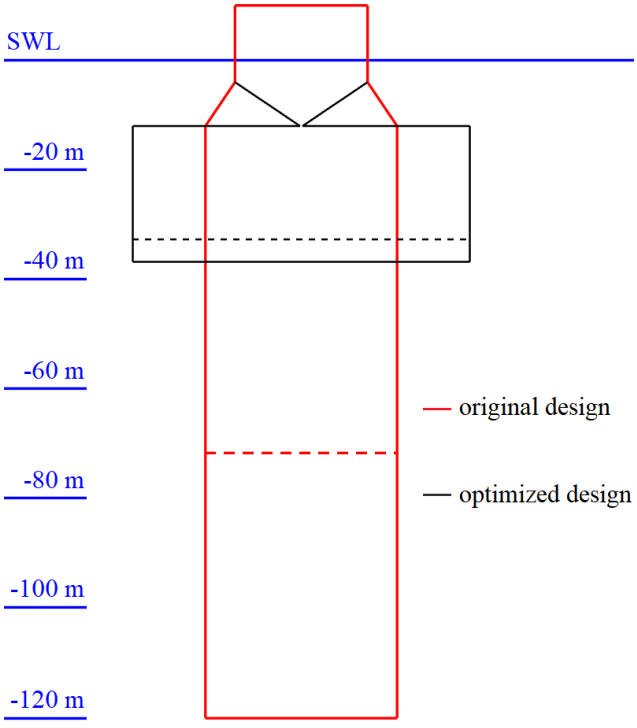

Figure 9. The optimized conceptual floater geometry in comparison to the original shape.

Table 7. Key figures of the optimized conceptual floater design.

Key figure	Value
Generation	166
Individual	51
x_1	0.115 m
x_2	2.653 m
x_3	16.525 m
x_4	0.001 m
x_5	3.0E-8 m
x_6	24.761 m
x_7	4.098 m
Ballast density	4.855E+03 kg/m^3
Wall thickness	0.0571 m
Draft	36.762 m
Max(tot. inclination angle)	10.000°
Max(hor. nacelle acceleration)	1.426 m/s^2
Mean(transl. motion)	28.394 m
f_1	93.9 m^3
Steel mass	7.373E+05 kg
Ballast mass	4.267E+06 kg

floater is, however, still significantly away from the minimum allowable draft of 15 m), the width of the bottom part of the support structure is enlarged, while the upper and middle parts are almost left out - leading to this significant constriction in the tapered part - and a very low ballast volume is obtained through a significantly increased ballast density, utilizing MagnaDense or high-density concrete as ballast material.

Overall, the shape of the optimized conceptual floater design resembles rather a submerged thick barge-type floater, hanging below the upper column element. This constriction in the tapered part is significant and would not directly be technically feasible, both from a manufacturing point of view and with respect to structural integrity. The reason for the current shape obtained is the connection of the upper column to the upper BC part, which, however, is, as well as the middle BC part, negligible. Thus, the tapered part could directly connect the end of the upper column with the top of the lower BC part, which is mainly purely the base column of the floater configuration. The change in required structure material would be not that significant; however, the related change in the displaced water volume has to be taken into account by adjusting the structure mass and by carefully evaluating the system performance due to the shifted center of buoyancy. This realization by means of a tapered section, however, comes with a large diameter change and corresponding large taper angle, which may be critical for both hydrodynamic load calculations and manufacturing, as discussed in more detail in Sect. 6. However, the structural issues due to the geometrical configuration of the optimized floater as presented in Fig. 9, or as well as due to the large diameter change when utilizing a tapered section, become void when eliminating the negligible upper and middle BC parts and connecting the upper column and lower BC part by means of a number of rigid slender braces or some tendons, in combination with plated partial bulkheads for load transfer, instead of using a tapered segment. These manufacturing solutions go beyond the conventional structural realization approach of welding cylindrical sections together, but they make the found optimized floater design solution feasible and are expected to represent similar system performance. The fitness of the floater solution proposed by the optimizer is underlined due to its similarity (with respect to the innovative structural realization approach) to the most novel and alternative solutions suggested by the research community, such as the Stiesdal's TetraSpar (Fig. 7(a)) (Borg et al., 2020; Stiesdal, 2019) or the Hexafloat by Saipem (Fig. 7(b)) (Ribuot, 2019; Richard, 2019).

5.4 Performance of the optimized system in different environmental conditions

With the conceptual design solution for the innovative floating offshore wind turbine platform obtained from the optimization run, finally, the DLCs that are selected for the preprocessing automated system simulations for choosing the most critical DLC (as presented in Sect. 4.1) are rerun to check whether a shift in the most critical DLC happens. The criticality is again assessed by evaluating the fully coupled system performance criteria (maximum total inclination angle, maximum horizontal nacelle acceleration, and mean translational motion) and analyzing the corresponding constraints g_{15} to g_{17}. The highest values and corresponding DLC simulation cases, as well as the values obtained with the selected DLC 1.6 at rated wind speed with wind seed number 11 and yaw misalignment angle of 8°, are presented in Table 8.

For the design solution from the optimization run, there is a shift in the criticality of the DLCs observed. The smallest change in the order of criticality of the 54 environmental conditions happens in the horizontal nacelle acceleration. Still, the cases from DLC 1.6 at cut-out wind speed, as well as around rated wind speed, are most critical, but the DLC used within the iterative

Table 8. The highest values for the three performance parameters and corresponding DLC simulation cases, based on the optimized floating system.

Position	DLC	Wind speed	Wind seed	Yaw misalignment	Max(total inclination angle)
1	1.1	13.0 m/s	18	8°	12.061°
2	1.1	11.4 m/s	10	0°	12.011°
3	1.3	11.4 m/s	10	0°	12.011°
4	1.1	11.4 m/s	7	-8°	11.903°
5	1.3	11.4 m/s	7	-8°	11.903°
30	1.6	11.4 m/s	11	8°	10.000°

Position	DLC	Wind speed	Wind seed	Yaw misalignment	Max(horizontal nacelle acceleration)
1	1.6	25.0 m/s	17	8°	1.620 m/s^2
2	1.6	25.0 m/s	18	8°	1.618 m/s^2
3	1.6	25.0 m/s	13	-8°	1.550 m/s^2
4	1.6	25.0 m/s	16	0°	1.521 m/s^2
5	1.6	25.0 m/s	15	0°	1.480 m/s^2
10	1.6	11.4 m/s	11	8°	1.426 m/s^2

Position	DLC	Wind speed	Wind seed	Yaw misalignment	Mean(translational motion)
1	1.1	13.0 m/s	15	0°	31.564 m
2	1.1	11.4 m/s	9	0°	31.375 m
3	1.3	11.4 m/s	9	0°	31.375 m
4	1.1	13.0 m/s	17	8°	30.631 m
5	1.1	11.4 m/s	12	8°	30.337 m
22	1.6	11.4 m/s	11	8°	28.394 m

optimization algorithm is still among the first ten with an acceleration value that is almost 12% lower compared to the maximum obtained from all simulated DLCs. This, however, is itself still more than 17% below the maximum allowable horizontal nacelle acceleration and, hence, uncritical, which - on a side note - is not the case for the original floating spar-buoy wind turbine system. A significant increase in the resulting performance values and considerable change in the order of criticality of the environmental conditions is obtained for the mean translational motion. Here, the selected DLC for the optimization process drops down from the originally sixth position to the 22nd, while it is just 10% below the highest value achieved, which is still less than half of the maximum allowable value and, hence, again uncritical. However, the most sever shift in the criticality of the DLCs happens for the total inclination angle of the system. As indicated in Sect. 5.3, the maximum allowable value

is already reached in the environmental condition considered for the optimization approach. This DLC, however, is for the obtained optimized design solution no longer prevailing but just on the 30th position, meaning that 29 other environmental conditions (mostly from DLC 1.1 and DLC 1.3, as well as some others from DLC 1.6) exceed the specified upper limit by up to more than 20%. In these environmental conditions, the floater design obtained from the optimization run would have to stop operation, while the overall system stability is not expected to be critical, as commonly much higher values for a parked floating wind turbine system in extreme environmental conditions are acceptable, such as 15° considered by Hegseth et al. (2020). However, to avoid reduced system availability, the occurring changed criticality of the DLCs has to be addressed already during the optimization - by, for example, considering safety factors for such critical and design-driving performance criteria. Alternatively or additionally, the performance in all environmental conditions can be further improved by subsequent optimization of the currently unaltered mooring system. These options are discussed in more detail in Sect. 6.

6 Discussion

In addition to the results presented, analyzed, and discussed in Sect. 5, more details on these results are addressed in the following and further aspects are discussed.

First of all, the duration of the optimization simulations needs to be addressed. If an additional stop criterion based on a realistic convergence tolerance has been specified, not the full 10,000 simulations would have to be simulated as the convergence tolerance would have been reached maybe already after around 40 generations. Thus, the conceptual design study would have required maybe just less than a quarter of the actually spent time. However, even around 181 hours - which is more than a week - is still too long for just a conceptual design study. The reason behind the currently quite long time required does not lie in the multi-fidelity framework and fully modular optimization problem setup, but rather in the developmental stage of the numerical model for a floating wind turbine system. Thus, a 800 s load case simulation with a floating wind turbine in irregular sea state and with turbulent wind conditions takes about four and a half hours, which is about 20 times as much as the time to be simulated. This is a known issue and part of the current development work at Fraunhofer IWES. While for bottom-fixed wind turbine systems real-time capability of the numerical models based on MoWiT has already been achieved (Feja and Huhn, 2019), the optimization of the code for floating systems is still at an early stage of development. However, based on the experience with the bottom-fixed numerical wind turbine system models, it is expected to achieve as well real-time capability for floating numerical wind turbine system models based on MoWiT after some further advancements of the code. At that time, the full simulation of the specified optimization problem will just require about one and a half days. This would then be very promising both for conceptual design studies, as well as detailed design optimization tasks, which - due to the fully modular and multi-fidelity approach applied - can be realized with the same numerical modeling and optimization environment.

Based on the findings of the DLC simulations with the optimized conceptual floating wind turbine system design, it is recommended to take some safety factors for the maximum allowable performance values into account. If the horizontal nacelle acceleration would have been exceeded in some of the 54 environmental conditions, it would not have been that critical, as a maximum allowable value of up to 0.3 times the gravitational acceleration constant - and not only 0.2 times as applied - is

often accepted, as already mentioned in Sect. 2.3. The specific maximum allowable values for an operating floating offshore wind turbine system have to be provided by the turbine manufacturer or operator. Thus, maybe a higher inclination angle is still acceptable; however, if 10° are really the uppermost tolerated angle, a value of 8° or maximum 9° shall be used for the optimization constraint. A reduced maximum allowable total inclination angle can as well afterwards be applied in the post-processing of the results and, this way, a floater design performing well in all 54 environmental conditions can be obtained. The downside of this approach, however, is that a larger structure material volume would be required and that this design would not represent an optimized solution. A profitable option, hence, is to adjust the - currently excluded and unchanged - mooring system properties and layout design. By modifying these in a subsequent optimization task, the optimized floater design can be retained and at the same time the performance of the floating offshore wind turbine system in all considered environmental conditions improved - in this case especially the system inclination. Apart from the considered 54 environmental conditions, however, the optimized floating offshore wind turbine system design has to prove to withstand any potential environmental and operational condition during its design life. Thus, for a subsequent more realistic and detailed design analysis, the entire set of DLCs recommended by standards has to be considered - at least in the pre-selection and final reassessment of the selected critical load case. The full set of DLCs should consider more realistic environmental conditions by accounting for various natural periods per considered sea state, utilize longer simulation times to capture the low frequency dynamics of the floating wind turbine system, and include also load cases with occurrence of a fault - such as grid loss - or with other transient loads - due to, for example, gusts - which might cause high accelerations and extreme loads.

Considering the wide design space - especially the broad allowable value ranges for the structural diameters - and the extreme environmental conditions, included in the DLC simulations, some refinements in the model with respect to the hydrodynamic calculations are suggested.

- For an accurate representation of the hydrodynamic loads on the floating structure, the hydrodynamic coefficients have to be recalculated for each specific diameter. While the horizontal added mass coefficient, as well as the total inertia force, are already determined in dependency of the actual structural diameter and wave number, as the MacCamy-Fuchs approach is applied for each column element separately, the horizontal drag coefficient is currently not altered from the original value of 0.6. This is a valid assumption for large diameters already at low flow velocities; however, for small diameter structures, which can occur within the optimization algorithm, an around twice as large horizontal drag coefficient might be applicable (Clauss et al., 1992). In the vertical (heave) direction, both added mass and drag coefficients are currently unchanged, while a vertical Froude-Krylov excitation force is considered, accounting for the difference between UC diameter and the diameter at the floater base. Especially for geometries with large diameter changes, as well as with large diameters, which can be regarded as heave plates, the hydrodynamic coefficients will differ from the original values for a continuous cylinder as the OC3 phase IV spar-buoy. Furthermore, the vertical Froude-Krylov excitation force would have to be adjusted to the specific geometry, when the lower BC part is connected by means of trusses or tendons to the upper column, to account for the differences between each upper and lower surfaces. Both - changes in the hydrodynamic coefficients in heave direction and adjusted vertical Froude-Krylov excitation force - will mainly affect the heave motion of the floating system, as well as the roll and pitch motions in some respect. With

the geometry obtained from the optimization, however, it is expected to experience less strong system responses if the hydrodynamic coefficients are adjusted accordingly - which would benefit, for example, the system inclination - while the system responses will increase slightly if the vertical Froude-Krylov excitation force is determined accurately for the considered geometry.

- For more extreme environmental conditions with extreme waves and similar structures as obtained with the optimization run, which tend to have a large diameter directly at or close to the top of the BC, the event that the upper surface of such a large diameter cylinder becomes dry has to be accounted for when calculating the added mass and damping coefficients in order to not overestimate the heave and pitch added mass and, thus, to not underestimate the horizontal nacelle acceleration in case of more energetic sea states. Furthermore, having a horizontal surface close to the water surface - in the presented settings with a minimum distance of 12 m - could be as well critical structurally or maybe due to the impossibility of common service vessels to approach the wind turbine. However, it has to be noted that it is aimed to establish a conceptual innovative floating platform design optimized with respect to the hydrodynamics. This, then, needs to be compromised imposing other prevailing constraints, such as structural limits - as discussed later in more detail again - or accessibility, for which, for example, walk-to-work solutions with a gangway can be exploited.

- The applied MacCamy-Fuchs approach is in principle just valid for cylinders with vertical walls and not for cylinders with abrupt changes of diameters, leading to conical sections or even large horizontal surfaces anywhere along the column (the latter one, however, is considered again by means of the vertical Froude-Krylov excitation force, as discussed previously). If the MacCamy-Fuchs approach is applied to conical structures, the wave load from especially waves with low periods will be underestimated. This could be in the order of magnitude of up to 8% or 14% for a cone angle of around 6.7° or 12.2°, respectively, and could affect wave periods of 3 s to 6 s or 3.5 s to 7 s, according to investigations on a tapered bottom-fixed offshore wind turbine support structure (Leimeister, 2019). Thus, this potential underestimation of the hydrodynamic loading is mostly relevant for the environmental conditions of DLC 1.1, as well as for the below and at rated wind speed cases of DLC 1.3. For the design solution proposed in Sect. 5.3, in which the bottom end of the upper column is directly connected with the large diameter lower BC part, the taper angle would amount 32°. Any hydrodynamic calculations based on the MacCamy-Fuchs approach would no longer be meaningful if the design solution is realized by means of a solid tapered part. Thus, the alternative suggestion of having instead a number of rigid slender braces would be favored. In order to ensure valid computation of the hydrodynamics already within the optimization approach, another constraint on the maximum taper angle shall be added, as implemented with a limit of 10° by Hegseth et al. (2020). This aspect is, however, less critical when allowing for different structural solutions - as done in this conceptual design study - where trusses or tendons prevent any utilization of strongly tapered sections.

Expectedly and as addressed and discussed in Sects. 5.2 and 5.3, the geometrical configurations of the potential (Fig. 6) and optimized (Fig. 9) innovative floater designs may not be technically feasible from a structural integrity and manufacturability point of view, adopting the standard manufacturing solutions. For obtaining a high detail structural design, further localized analyses and assessments regarding the manufacturability have to be performed subsequently. However, structural integrity

checks for buckling or stress concentration and for accounting for a realistic and adjustable base and lid thickness, which is currently just set to a fixed marginal value, can - due to the multi-fidelity character of the problem setup and framework - as well directly be integrated in the definition of the optimization problem for the subsequent detailed design study. Nonetheless, based on the assumptions and focus of this study, which is on a conceptual design development, as well as hydrodynamic and system-level analyses, a significantly improved and more cost-efficient floater with a highly innovative shape can be achieved. This is as well feasible when considering different structural realization approaches, such as braces and truss structures or tendons, as already used in the oil and gas industry (Fig. 1(a)) (Chen et al., 2017; Perry et al., 2007; Bangs et al., 2002) or utilized in innovative floater concepts (Fig. 7) (Richard, 2019; Stiesdal, 2019), instead of following purely the conventional structural approach of welding cylindrical and tapered sections together.

Finally and admittedly, for really considering an optimization of the wind turbine system cost, the ratio of CapEx (Capital Expenditure) to AEP (Annual Energy Production) or even the LCoE, which additionally takes OpEx (Operational Expenditure) - and sometimes also costs of decommissioning - into account, would have to be considered to be minimized. This way, a real trade-off between saved material costs, changed expenditure of manufacturing and maintenance of the system, and different system performance, and, hence, affected AEP can be found. However, this requires a more holistic and complex approach, considering annual environmental distributions at the location of interest, calculations for the full life-time of the system, as well as knowledge of possible manufacturing processes and related costs. The fully modular and multi-fidelity numerical modeling and optimization environment facilitates further extension of the present work to take into account these steps and aspects in the future.

7 Conclusions

In this paper, an automated optimization approach is applied to a spar-type floating offshore wind turbine system in order to develop a conceptual innovative floating platform design, which is optimized with respect to the change in hydrodynamics and their impact on the main system performance, while structural, manufacturability, or other constraints are not considered, whereas other advancements are facilitated. This approach, following a freer optimization formulation, is taken in order to be able to explore novel design spaces which can be better from a hydrodynamic point of view and show potential for more cost-efficient design solutions, but may require novel structural approaches, as actively investigated by the community (e.g. Stiesdal's TetraSpar and Saipem's Hexafloat). The application is based on the OC3 phase IV reference spar-buoy floating offshore wind turbine system. This, however, is modified by dividing the spar-buoy base column into three distinct partitions, so that sufficient buoyancy, as well as a deep center of gravity can be obtained. Furthermore, the wall thickness is adjusted based on a common ratio of the support structure's structural mass to the displaced mass of water. The optimization focuses on the minimization of the steel volume of the floater, which represents an approximation of the CapEx of the floating platform. In addition, constraints regarding the outer dimensions (meaning the allowable value ranges of the design variables), the global fully coupled system performance, the system draft, the ballast, and the geometric integrity are defined, whereby advanced features - such as alternative ballast materials or novel structural approaches - are incorporated in the definition of the value

ranges of the design variables and ballast density. Having selected, based on preprocessing automated system simulations, one DLC which is most critical for the constrained system performance criteria, the iterative optimization algorithm run is performed, utilizing the Python-Modelica framework for automated simulation and optimization, as well as using the genetic algorithm NSGAII as optimizer. The analysis of the optimization simulation results shows that the individuals which comply with all prescribed constraints aggregate as for their objective function values to an asymptote. The applied iterative optimization algorithm presented in this study yields a conceptual floating support structure design, which has a by more than 31% reduced structure material volume compared to the original floating platform, meets all global performance criteria for the considered critical DLC, has an overall draft of 36.8 m, utilizes MagnaDense or high-density concrete as ballast material, and resembles a submerged thick barge-type floater. Based on the applied hydrodynamic and system-level analyses an optimized initial innovative floater design is obtained, which has to be further refined by incorporating structural checks into the optimization process, but can be realized by means of alternative structural approaches, which utilize trusses or tendons instead of solely welding cylindrical sections together. Due to the fully modular and multi-fidelity character of the numerical modeling and optimization environment, the same framework can be utilized for a detailed design development and optimization, which is based on manufacturers' feedback on potential structural realization approaches, includes structural checks, and potentially utilizes more detailed hydrodynamic calculations as well.

Appendix A: Main properties of the OC3 phase IV floating offshore wind turbine system

The OC3 phase IV floating offshore wind turbine system consists of the NREL (National Renewable Energy Laboratory) 5 MW reference wind turbine (Jonkman et al., 2009), an offshore adapted tower, the spar-buoy floater, and three evenly spaced catenary mooring lines (Jonkman, 2010). The main properties of the floating wind turbine system, which is designed for a water depth of 320.0 m, are summarized in Table A1. This OC3 phase IV spar-buoy floating wind turbine system was defined as a reference design for code-to-code verifications and code-to-experiments validation and, hence, was not necessarily yet optimized.

Table A1. Main properties of the OC3 phase IV floating wind turbine system (Jonkman, 2010; Jonkman et al., 2009).

Wind turbine		**Offshore adapted tower**	
Rated power	5 MW	Top elevation above SWL[†]	87.6 m
Rotor diameter	126.0 m	Bottom elevation above SWL[†]	10.0 m
Hub height	90.0 m	Top diameter	3.87 m
Cut-in wind speed	3.0 m/s	Bottom diameter	6.5 m
Rated wind speed	11.4 m/s	Top wall thickness	0.019 m
Cut-out wind speed	25.0 m/s	Bottom wall thickness	0.027 m
RNA[*] mass	350,000 kg	Structural mass	249,718 kg

Spar-buoy floater		**Mooring lines**	
Elevation range of upper column	4.0 m below SWL[†] to 10.0 m above SWL[†]	Line length	902.2 m
Elevation range of base column	120.0 m to 12.0 m below SWL[†]	Line diameter	0.09 m
Upper column diameter	6.5 m	Fairlead position below SWL[†]	70.0 m
Base column diameter	9.4 m	Anchor position below SWL[†]	320.0 m
Mass including ballast	7,466,330 kg	Radius to anchor from floater centerline	853.87 m

[*] rotor-nacelle assembly

[†] still water level

Author contributions. ML: Conceptualization, Data curation, Methodology, Software, Validation, Formal analysis, Investigation, Project administration, Visualization, Writing - original draft, Writing - review; MC: Conceptualization, Methodology, Supervision, Writing - review & editing; AK: Supervision, Writing - review & editing, Funding acquisition.

Competing interests. The authors declare that they have no conflict of interest.

Acknowledgements. This work was partially supported by grant EP/L016303/1 for Cranfield University, University of Oxford and University of Strathclyde, Centre for Doctoral Training in Renewable Energy Marine Structures - REMS (http://www.remscdt.ac.uk/) from the UK Engineering and Physical Sciences Research Council (EPSRC) and the German Fraunhofer Institute for Wind Energy Systems (Fraunhofer IWES).

References

Bachynski, E. E.: Fixed and Floating Offshore Wind Turbine Support Structures, in: Offshore Wind Energy Technology, edited by Anaya-Lara, O., Tande, J. O., Uhlen, K., and Merz, K., pp. 103–142, Wiley, Hoboken, NJ, https://doi.org/10.1002/9781119097808.ch4, 2018.

Bachynski, E. E. and Moan, T.: Design considerations for tension leg platform wind turbines, Marine Structures, 29, 89–114, https://doi.org/10.1016/j.marstruc.2012.09.001, 2012.

Bachynski, E. E., Etemaddar, M., Kvittem, M. I., Luan, C., and Moan, T.: Dynamic Analysis of Floating Wind Turbines During Pitch Actuator Fault, Grid Loss, and Shutdown, Energy Procedia, 35, 210–222, https://doi.org/10.1016/j.egypro.2013.07.174, 2013.

Bangs, A. S., Miettinen, J. A., Silvola, I., Mikkola, T., and Beattie, S. M.: Design of the Truss Spars for the Nansen/Boomvang Field Development, in: Proceedings of the Offshore Technology Conference, Offshore Technology Conference, https://doi.org/10.4043/14090-MS, 2002.

Barbanti, G., Marino, E., and Borri, C.: Mooring System Optimization for a Spar-Buoy Wind Turbine in Rough Wind and Sea Conditions, in: Proceedings of the XV Conference of the Italian Association for Wind Engineering, edited by Ricciardelli, F. and Avossa, A. M., vol. 27 of *Lecture Notes in Civil Engineering*, pp. 87–98, Springer International Publishing, Cham, https://doi.org/10.1007/978-3-030-12815-9_7, 2019.

Berthelsen, P. A., Fylling, I., Vita, L., and Paulsen, U. S.: Conceptual Design of a Floating Support Structure and Mooring System for a Vertical Axis Wind Turbine, in: Proceedings of the ASME 31st International Conference on Ocean, Offshore and Arctic Engineering, pp. 259–268, American Society of Mechanical Engineers, New York, N.Y., https://doi.org/10.1115/OMAE2012-83335, 2012.

Borg, M., Walkusch Jensen, M., Urquhart, S., Andersen, M. T., Thomsen, J. B., and Stiesdal, H.: Technical Definition of the TetraSpar Demonstrator Floating Wind Turbine Foundation, Energies, 13, 4911, https://doi.org/10.3390/en13184911, 2020.

Butcher, N.: The Steel Tariff and Construction Cost: Putting It Into Context, Archinect, News, https://archinect.com/news/article/150058852/the-steel-tariff-and-construction-cost-putting-it-into-context, 2018.

Butterfield, S., Musial, W., Jonkman, J., and Sclavounos, P.: Engineering Challenges for Floating Offshore Wind Turbines: Conference Paper NREL/CP-500-38776, Proceedings of the European Offshore Wind Conference 2005, 26-28 October, Copenhagen, Denmark, 2007.

Chen, D., Gao, P., Huang, S., Fan, K., Zhuang, N., and Liao, Y.: Dynamic response and mooring optimization of spar-type substructure under combined action of wind, wave, and current, Journal of Renewable and Sustainable Energy, 9, 063 307, https://doi.org/10.1063/1.5017228, 2017.

Choi, E., Han, C., Kim, H., and Park, S.: Optimal design of floating substructures for spar-type wind turbine systems, Wind and Structures, 18, 253–265, https://doi.org/10.12989/was.2014.18.3.253, 2014.

Clauss, G., Lehmann, E., and Östergaard, C.: Offshore Structures: Volume I: Conceptual Design and Hydromechanics, Springer London, London, https://doi.org/10.1007/978-1-4471-3193-9, 1992.

Ding, Q., Li, C., Li, B., Hao, W., and Ye, Z.: Research on the Influence of Helical Strakes and Its Parameters on Dynamic Response of Platform of Floating Wind Turbine Based on Optimization Method of Orthogonal Design, Journal of Solar Energy Engineering, 139, 800, https://doi.org/10.1115/1.4037091, 2017a.

Ding, Q., Li, C., Ye, Z., Zhou, G., and Wang, D.: Research on Optimization for Dynamic Response of Platform of Floating Wind Turbine, Taiyangneng Xuebao/Acta Energiae Solaris Sinica, 38, 1405–1414, 2017b.

DNV GL AS: Loads and site conditions for wind turbines, vol. DNVGL-ST-0437, DNV GL AS, november 2016 edn., 2016.

DNV GL AS: Floating wind turbine structures, vol. DNVGL-ST-0119, DNV GL AS, july 2018 edn., 2018.

Dou, S., Pegalajar-Jurado, A., Wang, S., Bredmose, H., and Stolpe, M.: Optimization of floating wind turbine support structures using frequency-domain analysis and analytical gradients, Journal of Physics: Conference Series, 1618, 042 028, https://doi.org/10.1088/1742-6596/1618/4/042028, 2020.

European Wind Energy Association: Deep Water: The next step for offshore wind energy, EWEA, Brussels, Belgium, www.ewea.org/report/deep-water, 2013.

Feja, P. and Huhn, M.: Real Time Simulation of Wind Turbines for HiL Testing with MoWiT, in: Wind Energy Science Conference 2019 (WESC 2019), Zenodo, https://doi.org/10.5281/zenodo.3518727, 2019.

Future Power Technology: Floating foundations are the future of deeper offshore wind, Future Power Technology, Comment, 2019.

Fylling, I. and Berthelsen, P. A.: WINDOPT: An Optimization Tool for Floating Support Structures for Deep Water Wind Turbines, in: Proceedings of the ASME 30th International Conference on Ocean, Offshore and Arctic Engineering, pp. 767–776, American Society of Mechanical Engineers, New York, N.Y., https://doi.org/10.1115/OMAE2011-49985, 2011.

Gao, J. and Sweetman, B.: Design optimization of hull size for spar-based floating offshore wind turbines, Journal of Ocean Engineering and Marine Energy, 4, 217–229, https://doi.org/10.1007/s40722-018-0117-y, 2018.

Grogan, T.: Steel, Aluminum Tariffs Will Hit Prices Hard Through Year End, Engineering News-Record, https://www.enr.com/articles/44200-steel-aluminum-tariffs-will-hit-prices-hard-through-year-end?v=preview, 2018.

He, J., Jin, X., Xie, S. Y., Le Cao, Lin, Y., and Wang, N.: Multi-body dynamics modeling and TMD optimization based on the improved AFSA for floating wind turbines, Renewable Energy, 141, 305–321, https://doi.org/10.1016/j.renene.2019.04.005, 2019.

Hegseth, J. M., Bachynski, E. E., and Martins, J. R.: Integrated design optimization of spar floating wind turbines, Marine Structures, 72, 102 771, https://doi.org/10.1016/j.marstruc.2020.102771, 2020.

Hirai, T., Sou, A., and Nihei, Y.: Wave Load Acting on Advanced Spar in Regular Waves, in: Proceedings of the ASME 37th International Conference on Ocean, Offshore and Arctic Engineering, American Society of Mechanical Engineers, New York, N.Y., https://doi.org/10.1115/OMAE2018-77821, 2018.

Huijs, F., Mikx, J., Savenije, F., and de Ridder, E.-J.: Integrated design of floater, mooring and control system for a semi-submersible floating wind turbine, in: Proceedings of the EWEA Offshore, 2013.

International Electrotechnical Commission: Wind energy generation systems - Part 3-2: Design requirements for floating offshore wind turbines, vol. IEC TS 61400-3-2:2019-04(en), International Electrotechnical Commission, Geneva, 1.0 edn., 2019a.

International Electrotechnical Commission: Wind energy generation systems - Part 3-1: Design requirements for fixed offshore wind turbines, vol. IEC 61400-3-1:2019-04(en), International Electrotechnical Commission, Geneva, 1.0 edn., 2019b.

James, R. and Ros, M. C.: Floating Offshore Wind: Market and Technology Review, Carbon Trust, UK, 2015.

Jonkman, J.: Definition of the Floating System for Phase IV of OC3, NREL/TP-500-47535, National Renewable Energy Laboratory, Golden, Colorado, https://doi.org/10.2172/979456, 2010.

Jonkman, J., Butterfield, S., Musial, W., and Scott, G.: Definition of a 5-MW Reference Wind Turbine for Offshore System Development, NREL/TP-500-38060, National Renewable Energy Laboratory, Golden, Colorado, https://doi.org/10.2172/947422, 2009.

Karimi, M., Hall, M., Buckham, B., and Crawford, C.: A multi-objective design optimization approach for floating offshore wind turbine support structures, Journal of Ocean Engineering and Marine Energy, 3, 69–87, https://doi.org/10.1007/s40722-016-0072-4, 2017.

Katsouris, G. and Marina, A.: Cost Modelling of Floating Wind Farms, ECN-E-15-078, 2016.

Kolios, A., Borg, M., and Hanak, D.: Reliability analysis of complex limit states of floating wind turbines, Journal of Energy Challenges and Mechanics, 2, 6–9, 2015.

Krieger, A., Ramachandran, G. K. V., Vita, L., Alonso, P. G., Almería, G. G., Berque, J., and Aguirre, G.: Deliverable D7.2 Design Basis: LIFES50+, 2015.

Lee, K. H.: Responses of floating wind turbines to wind and wave excitation, Master thesis, Massachusetts Institute of Technology, http://hdl.handle.net/1721.1/33564, 2005.

Lee, Y.-J., Ho, C.-Y., Huang, Z., and Wang, Y.-C.: Improvements on the output of a spar-type floating wind turbine influened by wave-induced oscillation, Journal of Taiwan Society of Naval Architects and Marine Engineers, 34, 55–62, 2015.

Leimeister, M.: Python-Modelica Framework for Automated Simulation and Optimization, in: Proceedings of the 13th International Modelica Conference, Linköping Electronic Conference Proceedings, pp. 51–58, Linköping University Electronic Press, https://doi.org/10.3384/ecp1915751, 2019.

Leimeister, M. and Thomas, P.: The OneWind Modelica Library for Floating Offshore Wind Turbine Simulations with Flexible Structures, in: Proceedings of the 12th International Modelica Conference, Linköping Electronic Conference Proceedings, pp. 633–642, Linköping University Electronic Press, https://doi.org/10.3384/ecp17132633, 2017.

Leimeister, M., Kolios, A., and Collu, M.: Critical review of floating support structures for offshore wind farm deployment, Journal of Physics: Conference Series, 1104, 012 007, https://doi.org/10.1088/1742-6596/1104/1/012007, 2018.

Leimeister, M., Spill, S., Dose, B., Foglia, A., Siegl, K., Karch, M., Heins, E., Schümann, B., Dührkop, J., and Hartmann, H.: TANDEM - Towards an Advanced Design of Large Monopiles: Schlussbericht, Technische Informationsbibliothek (TIB), Hannover, Germany, https://doi.org/10.2314/KXP:1678117404, 2019.

Leimeister, M., Kolios, A., and Collu, M.: Development and Verification of an Aero-Hydro-Servo-Elastic Coupled Model of Dynamics for FOWT, Based on the MoWiT Library, Energies, 13, 1974, https://doi.org/10.3390/en13081974, 2020a.

Leimeister, M., Kolios, A., Collu, M., and Thomas, P.: Design optimization of the OC3 phase IV floating spar-buoy, based on global limit states, Ocean Engineering, 202, 107 186, https://doi.org/10.1016/j.oceaneng.2020.107186, 2020b.

Leimeister, M., Kolios, A., and Collu, M.: Development of a Framework for Wind Turbine Design and Optimization, Modelling, 2, 105–128, https://doi.org/10.3390/modelling2010006, 2021.

LKAB Minerals: Non-hazardous material safety data sheet for MagnaDense, https://www.lkabminerals.com/wp-content/uploads/2019/02/MagnaDense-SDS-12-06INT-19-03.pdf, 2019.

Main(e) International Consulting LLC: Floating Offshore Wind Foundations: Industry Consortia and Projects in the United States, Europe and Japan: An Overview, 2013.

Mast, E., Rawlinson, R., and Sixtensson, C.: TKI Wind op Zee: Potential of floating offshore wind: Market study floating wind in the Netherlands, RVO (Netherlands Enterprise Agency), 2015.

Matha, D., Sandner, F., and Schlipf, D.: Efficient critical design load case identification for floating offshore wind turbines with a reduced nonlinear model, Journal of Physics: Conference Series, 555, 012 069, https://doi.org/10.1088/1742-6596/555/1/012069, 2014.

Matsuoka, R. and Yoshimoto, H.: Verification of Precision Concerning the Design of Advanced Spar Type Structure, Conference Proceedings The Japan Society of Naval Architects and Ocean Engineers, 20, 2015S–OS1–1, 2015.

Men, J., Yan, F., and Ma, Q.: An optimization for the mooring system of a 10-MW spar type floating wind turbine in time domain, in: Proceedings of the 29th International Ocean and Polar Engineering Conference, pp. 384–389, International Society of Offshore and Polar Engineers, 2019.

Mishra, S., Sahoo, S., and Das, M.: Genetic Algorithm: An Efficient Tool for Global Optimization, Advances in Computational Sciences and Technology, 10, 2201–2211, 2017.

Molins, C., Trubat, P., Gironella, X., and Campos, A.: Design Optimization for a Truncated Catenary Mooring System for Scale Model Test, Journal of Marine Science and Engineering, 3, 1362–1381, https://doi.org/10.3390/jmse3041362, 2015.

Nejad, A. R., Bachynski, E. E., and Moan, T.: On Tower Top Axial Acceleration and Drivetrain Responses in a Spar-Type Floating Wind Turbine, in: Proceedings of the ASME 36th International Conference on Ocean, Offshore and Arctic Engineering, American Society of Mechanical Engineers, New York, N.Y., https://doi.org/10.1115/OMAE2017-62314, 2017.

Ng, C. and Ran, L., eds.: Offshore wind farms: Technologies, design and operation, vol. number 92 of *Woodhead Publishing series in energy*, Elsevier WP Woodhead Publishing, Amsterdam and Boston and Cambridge and Heidelberg and London and New York and Oxford and Paris and San Diego and San Francisco, 2016.

Perry, M. J., Halkyard, J. E., and Koh, C. G.: Rapid Preliminary Design of Floating Offshore Structures Using a Modified Genetic Algorithm, in: Proceedings of the ASME 26th International Conference on Ocean, Offshore and Arctic Engineering, pp. 777–784, American Society of Mechanical Engineers, New York, N.Y., https://doi.org/10.1115/OMAE2007-29700, 2007.

Pham, T. D. and Shin, H.: A New Conceptual Design and Dynamic Analysis of a Spar-Type Offshore Wind Turbine Combined with a Moonpool, Energies, 12, 3737, https://doi.org/10.3390/en12193737, 2019.

Quest Floating Wind Energy: The Definitive Guide to Floating Wind Concepts, Quest Floating Wind Energy, 2020.

Ribuot, J.: HEXAFLOAT - Innovative Competitive Offshore Energy Production, in: MCE Deepwater Development 2019 (MCEDD 2019), https://mcedd.com/wp-content/uploads/2019/04/MCEDD-2019-Presentation-SAIPEM-18-March.pdf, 2019.

Richard, C.: Funds for Ireland's first floating demonstrator, Windpower Monthly, https://www.windpowermonthly.com/article/1579762/funds-irelands-first-floating-demonstrator, 2019.

Robertson, A., Jonkman, J., Masciola, M., Song, H., Goupee, A., Coulling, A., and Luan, C.: Definition of the Semisubmersible Floating System for Phase II of OC4, NREL/TP-5000-60601, National Renewable Energy Laboratory, Golden, Colorado, 2014.

Sandner, F., Schlipf, D., Matha, D., and Cheng, P. W.: Integrated Optimization of Floating Wind Turbine Systems, in: Proceedings of the ASME 33rd International Conference on Ocean, Offshore and Arctic Engineering, American Society of Mechanical Engineers, New York, N.Y., https://doi.org/10.1115/OMAE2014-24244, 2014.

Sclavounos, P., Tracy, C., and Lee, S.: Floating Offshore Wind Turbines: Responses in a Seastate Pareto Optimal Designs and Economic Assessment, in: Proceedings of the ASME 27th International Conference on Ocean, Offshore and Arctic Engineering, pp. 31–41, American Society of Mechanical Engineers, New York, N.Y., https://doi.org/10.1115/OMAE2008-57056, 2008.

Stiesdal, H.: TetraSpar and TetraBase: Industrialized Offshore Wind Turbine Foundations, Stiesdal Offshore Technology, https://www.stiesdal.com/material/2019/02/Stiesdal-Tetra-01.02.19.pdf, 2019.

Strobel, M., Vorpahl, F., Hillmann, C., Gu, X., Zuga, A., and Wihlfahrt, U.: The OnWind Modelica Library for OffshoreWind Turbines - Implementation and first results, in: Proceedings from the 8th International Modelica Conference, Linköping Electronic Conference Proceedings, pp. 603–609, Linköping University Electronic Press, https://doi.org/10.3384/ecp11063603, 2011.

Suzuki, K., Yamaguchi, H., Akase, M., Imakita, A., Ishihara, T., Fukumoto, Y., and Oyama, T.: Initial Design of Tension Leg Platform for Offshore Wind Farm, Journal of Fluid Science and Technology, 6, 372–381, https://doi.org/10.1299/jfst.6.372, 2011.

Tafazzoli, S., Shafaghat, R., and Alamian, R.: Optimization study of a catenary mooring system for a spar floating wind turbine based on its hydrodynamic responses, Proceedings of the Institution of Mechanical Engineers, Part M: Journal of Engineering for the Maritime Environment, 12, 1475090220917812, https://doi.org/10.1177/1475090220917812, 2020.

Thomas, P., Gu, X., Samlaus, R., Hillmann, C., and Wihlfahrt, U.: The OneWind Modelica Library for Wind Turbine Simulation with Flexible Structure - Modal Reduction Method in Modelica, in: Proceedings of the 10th International Modelica Conference, Linköping Electronic Conference Proceedings, pp. 939–948, Linköping University Electronic Press, https://doi.org/10.3384/ECP14096939, 2014.

Udoh, I. E.: A Concise Methodology for the Design of Statically-Equivalent Deep-Offshore Mooring Systems, in: Proceedings of the ASME 33rd International Conference on Ocean, Offshore and Arctic Engineering, American Society of Mechanical Engineers, New York, N.Y., https://doi.org/10.1115/OMAE2014-23054, 2014.

WindEurope: Floating Offshore Wind Vision Statement, vol. June 2017, WindEurope, Brussels, Belgium, 2017.

Wright, C., Yoshimoto, H., Wada, R., and Takagi, K.: Numerical Modelling of a Relatively Small Floating Body's Wave and Low Frequency Motion Response, Compared With Observational Data, in: Proceedings of the ASME 38th International Conference on Ocean, Offshore and Arctic Engineering, American Society of Mechanical Engineers, https://doi.org/10.1115/OMAE2019-96443, 2019.

Yamanaka, S., Hirai, T., Nihei, Y., and Sou, A.: Interaction Between Advanced Spar and Regular Waves, in: Proceedings of the ASME 36th International Conference on Ocean, Offshore and Arctic Engineering, American Society of Mechanical Engineers, New York, N.Y., https://doi.org/10.1115/OMAE2017-61788, 2017.

Yoshimoto, H. and Kamizawa, K.: Validation of the Motion Analysis Method of Floating Offshore Wind Turbines Using Observation Data Acquired by Full Scale Demonstration Project, in: Proceedings of the ASME 38th International Conference on Ocean, Offshore and Arctic Engineering, American Society of Mechanical Engineers, https://doi.org/10.1115/OMAE2019-95828, 2019.

Yoshimoto, H., Yoshida, H., and Kamizawa, K.: Validation of Applicability of Low Frequency Motion Analysis Theory Using Observation Data of Floating Offshore Substation, in: Proceedings of the ASME 37th International Conference on Ocean, Offshore and Arctic Engineering, American Society of Mechanical Engineers, New York, N.Y., https://doi.org/10.1115/OMAE2018-77201, 2018.

Zhu, H., Sueyoshi, M., Hu, C., and Yoshida, S.: A study on a floating type shrouded wind turbine: Design, modeling and analysis, Renewable Energy, 134, 1099–1113, https://doi.org/10.1016/j.renene.2018.09.028, 2019.